

A STUDY OF THERMALLY STIMULATED CHARGE EMISSION
AND THERMALLY STIMULATED LUMINESCENCE
FROM MgO SINGLE CRYSTALS

By

HOWARD CHARLES MOLLENKOPF
//

Bachelor of Science
North Texas State University
Denton, Texas
1964

Master of Science
North Texas State University
Denton, Texas
1967

Submitted to the Faculty of the Graduate College
of the Oklahoma State University
in partial fulfillment of the requirements
for the Degree of
DOCTOR OF PHILOSOPHY
May, 1973

Thesis
1973 D
M 726s
cop. 2

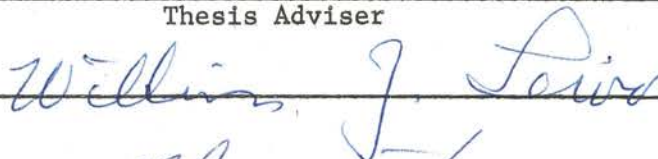
FEB 18 1974

A STUDY OF THERMALLY STIMULATED CHARGE EMISSION
AND THERMALLY STIMULATED LUMINESCENCE
FROM MgO SINGLE CRYSTALS

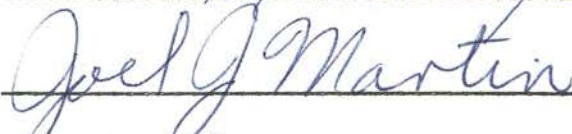
Thesis Approved:



Thesis Adviser









Dean of the Graduate College

873415

ACKNOWLEDGMENTS

The author is most grateful to Dr. E. E. Kohnke for his patience, supervision and guidance throughout the course of this research. Gratitude is also expressed to Dr. L. Halliburton for his contribution in obtaining the E.S.R. data that helped significantly with the correlation of the T.S.C.E. and the T.S.L., and also to Dr. W. A. Sibley for the use of his emission spectroscopy equipment. The author is also indebted to Dr. C. T. Butler for the supply of MgO crystals and their analysis and to Mr. Heinz Hall for his help with the design of the stainless steel high vacuum system and Mr. Wayne Adkins for his help with the glass components associated with both the gas and vacuum systems. The author wishes to express his appreciation to the Physics Department and the National Science Foundation for the research traineeship made available for the final two years of research. Last, but by no means least, he wishes to thank his wife, Ruth, for her patience, understanding and encouragement throughout this study.

TABLE OF CONTENTS

Chapter	Page
I. INTRODUCTION.	1
The Historical Development of Exoelectron Emission	1
Thermally Stimulated Luminescence and Exoelectron Emission	3
Applications of Exoelectron Emission	5
Scope of the Present Study	5
II. THE THEORY AND ANALYSIS OF THERMALLY STIMULATED EXOELEC- TRON EMISSION	8
Introduction	8
Models for T.S.C.E.	8
Activation Energy Analysis	11
III. EXPERIMENTAL DETAILS.	19
Introduction	19
Apparatus and Measuring Techniques	19
(1) Gas Counting	19
(2) High Vacuum Counting	24
(3) E.S.R. Spectrometer.	27
Observation of Materials Different From MgO.	27
MgO Samples and Their Preparation.	28
IV. EXPERIMENTAL RESULTS.	30
Introduction	30
Characteristic T.S.L. and T.S.C.E. Measurements.	30
Emission Spectroscopy.	30
Electron Spin Resonance.	30
T.S.L. Using a Blue and Red Sensitive Photomultiplier.	30
Gamma Irradiation Effects.	31
Bleaching Effects on T.S.L. and T.S.C.E.	31
T.S.C.E. Peak Intensity Changes.	31
Magnetic Field and Grid Voltage Effects on T.S.C.E..	31
V. DISCUSSION AND CONCLUSIONS.	59
T.S.L. and Hole Centers in MgO	59

TABLE OF CONTENTS (Continued)

Chapter	Page
Charge Emission From MgO	63
Activation Energy Analysis	65
Summary.	66
Suggestions for Further Study.	67
BIBLIOGRAPHY.	69

LIST OF TABLES

Table	Page
I. Information Pertaining to the Glow and Charge Emission Curves of Figures 8, 9, and 10	36
II. Summary of E.S.R., T.S.L., T.S.C.E. and Emission Spectro- scopy From MgO-6	40

LIST OF FIGURES

Figure	Page
1. Auger Model.	12
2. Simplified Model for T.S.C.E. and T.S.L.	14
3. Electron Trap Population C and Its Reduction During Heating.	17
4. Block Diagram of Gas Counting Equipment.	20
5. T.S.C.E. Gas Detection System.	21
6. Block Diagram of the High Vacuum Detection System.	25
7. Charge Detector and Associated Electronics	26
8. T.S.C.E. and T.S.L. From MgO-2	32
9. T.S.C.E. and T.S.L. From MgO-3	33
10. T.S.C.E. and T.S.L. From MgO-6	34
11. Spectral Distribution of MgO-6	37
12. E.S.R. From MgO-6.	39
13. T.S.L. From MgO-2 With an RCA-7102 Photomultiplier	41
14. T.S.L. From MgO-3 After Gamma Irradiation at 300°K and Ultraviolet Excitation Near 77°K	44
15. 546 Nanometer Bleaching of T.S.C.E. From MgO-6 at 300°K.	46
16. 546 Nanometer Bleaching of T.S.C.E. From MgO-6 Near 77°K	48
17. 546 Nanometer Bleaching of T.S.L. From MgO-6 Near 77°K	49
18. 254 Nanometer Re-excitation of T.S.C.E. From MgO-6	50
19. T.S.L. From MgO-6 After 254 Nanometer Excitation Near 77°K.	52
20. T.S.C.E. Intensity Changes in the Gas System	54
21. T.S.C.E. Intensity Changes in the Vacuum System.	56

CHAPTER I

INTRODUCTION

The Historical Development of Exoelectron Emission

It was observed in 1936 by Lewis and Burcham (1) that high background counts appeared in new GM counters. They attributed this to ionization phenomena accompanying the reaction of oxygen with the freshly abraded metals from which the counters were constructed. In the review article by Grunberg (2), it is noted that J. Kramer was the first to recognize the fact that the phenomena observed by Lewis and Burcham could be used to investigate metal surfaces. Kramer's work in 1950 dealt mainly with metals that were abraded prior to their investigation with a point counter (2). In a typical experiment, Kramer would place an abraded piece of metal under the counter anode and observe an emission of electrons that would decay with time. An experiment with Wood's metal led him to believe that the charge emission, that occurred as the sample changed phase from a melt by solidification, was associated with an exothermal process. Kramer then believed that all of the charge emissions he had observed were caused by exothermal processes and he termed electrons emitted in this manner "exoelectrons".

Grunberg and Wright (3) used visible light well above the photoelectric threshold to investigate abraded metal surfaces and thought that F'-centers (oxygen ion vacancies occupied by two electrons), which, when returning to the ground state, caused emission from shallow centers

near the oxidized surface. In 1961 Pimbley and Francis (4) applied Grunberg and Wright's method of excitation and observed exoelectron emission (E.E.E.) from abraded aluminum surfaces. They believed that the E.E.E. was governed by the vacancies produced in the metal by the abrading, and that these vacancies diffused to the surface where they released energy to electrons. If the energy of both the vacancy and the incident light were greater than the work function of the metal then this energy was responsible for the E.E.E. Later Scharmann, Seibert (5) and Ramsey (6) succeeded in proving that no E.E.E. occurs from Aluminum surfaces abraded in ultra-high vacuum. However, the increase of oxygen pressure caused the E.E.E. to reappear. Ramsey was also able to show that water vapor and oxygen are most important for the emission phenomena. Gesell, Arakawa and Collicott (7) observed E.E.E. during oxygen and water chemisorption on fresh Mg surfaces. They concluded that the energy necessary for E.E.E. comes from the reaction of O_2 or H_2O with a freshly exposed Mg surface.

Drenckhan, Gross and Glaefcke (8) were able to detect E.E.E. from oxidized silicon crystals bombarded with 1.5 Kev electrons in ultra-high vacuum. Subsequent removal of the thin oxide layer from the silicon crystals with the aid of argon ion bombardment in vacuum caused the E.E.E. to disappear. By assuming that E.E.E. only takes place if insulating surface layers are present, they predicted an emission model (9) where electrons receive their emission energy from an internal electric field produced by the incident high energy electrons. The incident electrons produce a positive surface charge and a negative space charge just below the surface that sets up the accelerating electric field for the E.E.E.

Hence, the term exoelectron emission continued in use for historical reasons and, in general, pertains to a small electron emission from a solid when the process by which electrons are excited over the surface barrier is not clearly related to external stimuli, such as photoemission, charged or metastable particles (secondary and Auger emission), field emission or to high temperature thermionic emission.

Thermally Stimulated Luminescence and Exoelectron Emission

At the time of the discovery of E.E.E., the theory of Thermally Stimulated Luminescence (T.S.L.) or simply thermoluminescence was well established. It was known that if ionizing radiation was used on certain ceramics or crystals that a charge transfer would take place. Subsequent heating of the material would then release the charge (e.g., electrons) at definite temperatures by way of the conduction band, with the possibility of recombination in radiationless transitions or recombination with empty traps, and the emission of photons (T.S.L.) characteristic of the trapping levels. The detection of the light intensity as a function of temperature is then referred to as a T.S.L. "glow curve". The T.S.L. glow curve can then be used to determine such trapping parameters as activation energy (10), attempt-to-escape frequencies (11), and trap density distributions (12). A good recent review of the various methods of analyzing T.S.L. is given by Kelly, Laubitz and Braunlich (13).

Lepper (14) was able to detect an individual E.E.E. glow curve from pure CaSO_4 and $\text{CaSO}_4:\text{Mn}$ by linearly raising the temperature of each specimen after ionizing irradiation, and observing the E.E.E. maxima near

200°C. He also observed a T.S.L. glow curve using the same heating schedule for $\text{CaSO}_4:\text{Mn}$, with the T.S.L. maximum appearing at the same temperature. This implied that the presence of Mn is necessary for the T.S.L. but not for the E.E.E. Novotney, Spurney, and Binova (15) also observed the T.S.L. and E.E.E. of pure CaSO_4 , $\text{CaSO}_4:\text{Mn}$ and $\text{CaSO}_4:\text{Pb}$. They varied the content of Mn and Pb and applied x-irradiation at room temperature to determine the optimum concentrations of each dopant necessary to maximize both the T.S.L. and the E.E.E. A reasonable consistency was obtained in both of the glow curve peak temperature positions and small differences (< 0.05 ev) existed between their calculated activation energies. This implied the same traps are important for both the E.E.E. and the T.S.L. processes.

In general, complete agreement between E.E.E. and T.S.L. is rare. Several reasons could be responsible for this, such as:

1. the electrons may be ejected during non-radiative transfer from one energy-state to another,
2. the wavelength of the T.S.L. may not be within the range of the spectral response of the P.M.T.,
3. the traps may exist completely on the surface and support only E.E.E. (i.e., no radiative recombination),
4. the traps may exist in the bulk of the material and support only T.S.L.

Although various hypotheses have been proposed to explain the emission phenomena, the detailed mechanism by which the electrons leave the crystal still remains unexplained. Holzapfel (16) assumed a quasi-stationary thermionic emission of electrons from a high speed Maxwell tail while Gapaindoshvily, Kortov (17), Bichevin and Kaambre (18),

Tolpygo, Tolpygo and Sheinkman (19) all suggest the Auger method as the mechanism necessary for the E.E.E. Kelly's (20) phenomenological theories of T.S.L. and Thermally Stimulated Conductivity (T.S.C.) have been recently extended to E.E.E. This extension implies that E.E.E. can have a marked effect on the magnitude of T.S.L., especially for thin films or specimens with a high surface-to-volume ratio.

Applications of Exoelectron Emission

One of the most recent applications of E.E.E. is in the field of dosimetry, where the terminology Thermally Stimulated Exoelectron Emission (T.S.E.E.) is used instead of E.E.E. Becker (21) has a complete review of this and also references the use of E.E.E. for imaging devices (E.E.E. "photography"), for investigating solid-state chemical reactions, or the study of the radiolysis of water, for geological and biophysical studies or as an ultrasensitive analytical method in metallographic or catalysis studies.

Scope of the Present Study

Bohun (22), Bohun and Kaambre (23) were among the first to point out that E.E.E. is definitely associated with color centers in ionic crystals. They simultaneously detected both E.E.E. and T.S.L. from colored alkali halide crystals, both pure and doped, and have indicated that the charge emission and the luminescence are associated with the color centers (i.e., F centers-electrons trapped in anion vacancies). Most of the E.E.E. study concerning color centers or radiation damage has been concerned with the alkali halides and understandably so, for more is known about these materials, especially with respect to color

centers. Similarly, a fair amount of experimentation has been performed on the alkaline earth oxides. MgO is a good example of this class of oxides, having a simple cubic lattice structure with a band gap of 8.7 ev (24). It has received relatively little attention concerning E.E.E. compared to the E.S.R., optical absorption, luminescence, T.S.L., T.S.C. and color center experimentation that has been performed on both pure and doped MgO single crystals. Spin resonance studies have shown that V^- (Mg^{2+} vacancy occupied by a hole), V^0 (Mg^{2+} vacancy occupied by two holes), V_{OH} (V^- center with H trapped in the Mg^{2+} vacancy), F^+ (O^- vacancy occupied by one electron) and F (O^- vacancy occupied by two electrons) bulk color centers are the most predominant in irradiated MgO single crystals (25, 26). The concentration of each type of color center depends primarily on the source (U.V., γ , electron or neutron) and intensity of irradiation, the type and concentration of impurities, and the method used in growing the crystal.

Krylova (27) has indicated that after bombarding a variety of oxides (Al_2O_3 , SiO_2 , zeolite, MgO, ZnO, TiO_2 , ZrO_2 , Cu_2O and NiO) with electrons, that E.E.E. peaks coincide with the maxima of thermal desorption rates for water and oxygen. Recently Nelson, Hale and Harmsworth (28) have identified the O_2^- ion adsorbed on powdered MgO after U.V. and γ irradiations at a reduced oxygen pressure. They associated the adsorbed O_2^- ions with surface F^+ and V^- color centers, and another unidentified site with the aid of E.S.R. spectra. Wong and Lunsford (29) have identified an E.S.R. spectrum produced by O^- ions on powdered MgO, that had been heat treated in vacuum and then U.V. irradiated in the presence of hydrogen (50 Torr). They predicted a crystal field stabilization energy of 0.65 ev for the O^- ion trapped in an O^- ion vacancy on the surface of

the MgO.

The E.S.R. studies of bulk color centers are more thoroughly established for MgO than those of the surface. This is to be expected for bulk centers exist at higher concentrations and can be examined in a more stable state in pure single crystals. In general, recent E.S.R. and T.S.L. experimentation (30) have indicated that the V^- center interacts with the Fe^{2+} and Cr^{2+} impurities near $100^{\circ}C$. Similar studies involving E.S.R., luminescence (31), and T.S.L. (32) imply that the V^- center interacts with Cr^{2+} near $100^{\circ}C$.

Crawford and Mallard (33) have implied from Thermal Electric Power (T.E.P.) and T.S.C. measurements that the major conduction in γ -irradiated MgO crystals is by holes above $100^{\circ}C$ and by electrons below this temperature.

It is thought in general that more than one physical method will have to be used in order to explain the mechanism of Thermally Stimulated Charge Emission (T.S.C.E.). The terminology T.S.C.E. is more appropriate since Gordon, Scharmann, and Seibert (34), Maenhout and De Muer (35) have detected ions as well as electrons in their charge emission experimentation. It is then the intent of the research reported here to:

1. establish a model for T.S.L. in the MgO single crystals used with the aid of E.S.R.,
2. determine the nature of the charge emission (i.e., ions or electrons) and the energy with which the charge is released and,
3. correlate these data to better establish the mechanism of T.S.C.E. from MgO.

CHAPTER II

THE THEORY AND ANALYSIS OF THERMALLY STIMULATED CHARGE EMISSION

Introduction

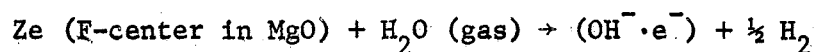
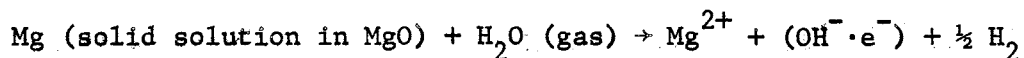
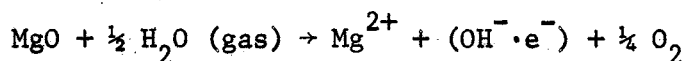
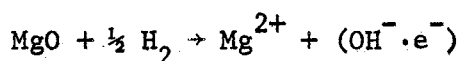
This chapter consists of the description of three basic models to explain the phenomena of charge emission and the necessary assumptions for applying some activation energy analysis to the charge emission and the T.S.L. glow peaks. The three models are the Maxwell tail theory (45, 46), the direct emission from surface traps (48, 49, 27), and the Auger effect (18, 19, 47). Following this, two methods of activation energy analysis will be discussed in conjunction with the necessary assumptions for their use on both the charge emission and the T.S.L. These two activation energy techniques consist of the initial-rise (10) method and the Balarin-Zetsche (40) method.

Models for Charge Emission

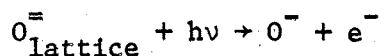
The Maxwell tail theory refers to those electrons of the Maxwell tail thermally emitted from traps into the conduction band and having sufficient kinetic energy to overcome the surface potential barrier. That electron emission in a high vacuum does have a Maxwellian energy distribution was shown by Kriegeis and Scharmann (36). This model should then be more applicable at temperatures above room temperature and for low electron affinity materials. Holzapfel (16) has theorized that work

functions greater than 1 ev will alter charge emission peaks above room temperature, while peaks below this temperature are inhibited more by even smaller work functions. By assuming the Maxwell tail theory or the "quasi stationary thermionic emission" model, he was able to show that increasing work functions caused charged emission peaks to shift to higher temperatures.

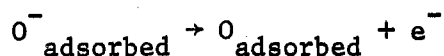
Since the work function of any material takes into consideration the surface structure as well as the chemisorbed--or to a lesser extent--the physically adsorbed foreign gas, then the affects of this sorption on charge emission have to be considered. The release of charge from surface states produced by sorption is referred to as direct emission. Krylova (27), Krylova et al. (48, 49) have noted that by bombarding oxide powders with 1.5 Kev electrons in a high vacuum, there is always a release of H_2O and O_2 with subsequent heating at the same time that charge emission occurs. From mass spectrometer analysis they conclude that the charge release comes from a consequence of H_2O desorption at low temperature and OH^- at high temperatures, with OH^- groups acting as localized centers for electron traps (50, 51). They suggested the following mechanisms for donor $OH^- \cdot e^-$ centers:



Krylova (27) has also proposed that



where lattice oxygen is transferred to adsorbed oxygen or chemically adsorbed oxygen to a physically adsorbed state. The fact that the highest rate of evolution of adsorbed oxygen is observed for ZnO and Al_2O_3 in the 140 to 160°C range, and that Krylova observed strong charge emission in this same temperature interval for a variety of oxide powders, led him to believe that the following processes may take place:



implying electron emission and partial desorption of oxygen simultaneously.

Similarly Kriegeis and Scharmann (37) have observed two main charge emission peaks at 115°C and 160°C in high vacuum from BaSO_4 powder. After annealing the powder at 300°C in high vacuum and then exciting the material with 2.5 Kev electrons, the 160°C peak was diminished significantly. O_2 sorption would bring the 160°C peak back with some decrease in the 115°C peak. H_2O adsorption prior to irradiation seemed to lower the 115°C peak only. Since all of the vacuum work mentioned above involves excitation energies up to 2.5 Kev, the question remains to be answered whether or not the excitation causes radiolysis of water on the material surface producing hydroxyl groups that would act as surface traps for the excess charge produced by the irradiation. This excess charge might then be thermally released with subsequent heating producing direct emission from the surface traps.

In view of the Maxwell tail theory and the direct emission models, it is surprising that charge can be thermally released from materials

with any measurable energy at all, especially within 500°C of room temperature. However, average emission energies of 1.1 eV have been reported by Kriegeis and Scharmann (36) from their Maxwellian energy distribution studies. The Auger effect model is suitable for explaining such emission energies. If the material under observation has a large band gap, with respect to its electron affinity ($E_g \gg x$), and if defect holes exist that can be thermally released with subsequent heating, then the Auger model is applicable. The energy released by the recombination of the thermally released hole with a trapped electron can be transferred to another electron localized at a nearby impurity, to a hydroxyl group, or to an adsorbed gas ion. The energy released by the hole-electron recombination is then a radiationless type recombination energy that can be transferred from the vicinity of the hole-electron pair to a nearby trapped charge. If the trapped charge is an electron near the surface of the material, then the electron can be emitted with kinetic energy E_{Kin}^- . Therefore, it is a competitive process with the hole-electron recombination luminescence that might also exist in the same temperature region. Figure 1 is an illustration of the Auger effect model with thermally activated holes recombining either with (1) a doubly occupied charge center, (2) with singly occupied charge centers, or (3) with different occupied charge centers.

Activation Energy Analysis

The study of thermal excitation processes involves the transfer of electrons and/or holes from forbidden band energy levels into the conduction band or the valence band respectively. It has been shown from several theoretical investigations (52, 53, 54, 55, 56, 57) that the

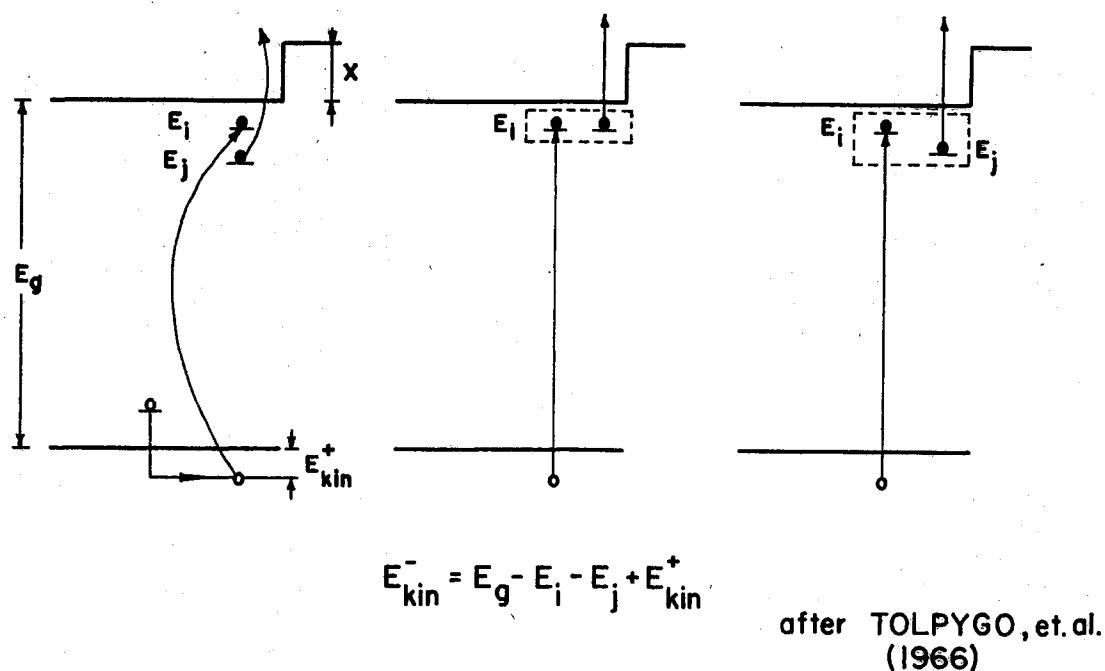


Figure 1. Auger Model

probability per unit time of an electron (hole) escaping from a trap of energy E below (above) the conduction band (valence band) at temperature T can be expressed by

$$P = K_0(E, T) e^{-E/kT} \quad (1)$$

where $K_0(E, T)$ is a rough measure for the collision frequency of trapped electrons and surrounding lattice atoms. K_0 is usually referred to as the frequency factor, if the trap is regarded as a potential box, that expresses the product of the frequency of the electron oscillation and the reflection coefficient (58). In general, K_0 is dependent upon E , charge distribution, bonding characteristics and temperatures, however,

only the order of magnitude is usually of interest and K_0 is generally considered a constant. Its experimental value is usually within a few orders of magnitude of the Debye frequency ($\approx 10^{13} \text{ sec}^{-1}$), the optical vibration frequency of a crystal. The factor $e^{-E/kT}$, where k is Boltzmann's constant, represents the probability that the electron (hole) has in overcoming the potential barrier of energy E .

Figure 2 illustrates the processes of T.S.C.E. and T.S.L. as suggested by others from a simplified energy level scheme of a material after excitation. Here, transitions between the traps H , that have been filled by excitation, the conduction band and subsequent emission into the gas or vacuum and the recombination centers A , are considered. Figure 2 and some simplifying assumptions about the trapped charge and the detrapping process that takes place with subsequent heating will help overcome mathematical difficulties that will allow for the evaluation of the activation energy E . The assumptions are:

- (1) The charge transfer that contributes to a glow peak or the charge emission comes from traps at a single energy level.
- (2) The charge emission has a Maxwellian energy distribution.
- (3) There is no retrapping of charge (i.e., δ the trapping coefficient = 0).
- (4) The detrapping rate is proportional to the instantaneous concentration of trapped charge.
- (5) The phenomenological time rate equation is applicable where

$$-\frac{dh}{dt} = Ph = h K_0 e^{-E/kT} \quad (2)$$

and $h(T)$ represents the concentration of trapped charge at a temperature

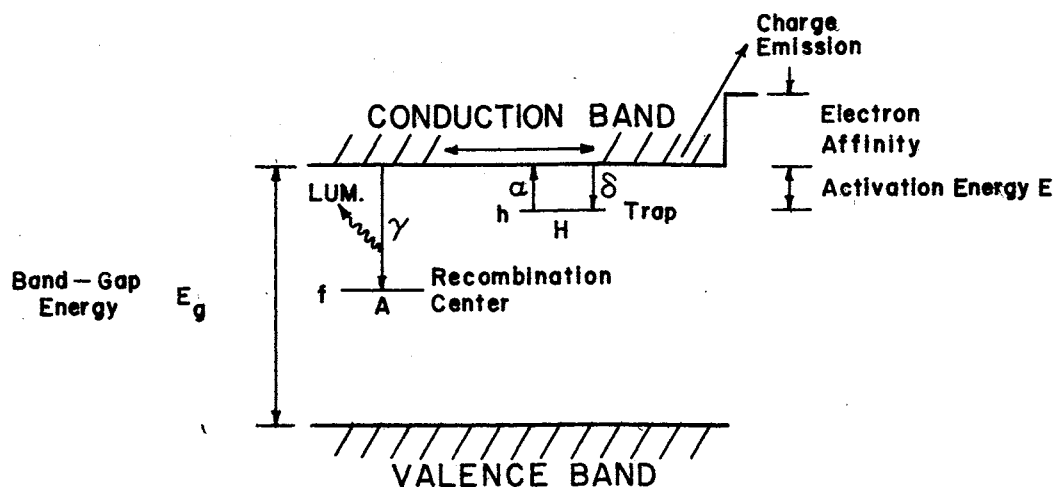


Figure 2. Simplified Model for T.S.C.E. and T.S.L.

T much less than that at which the peak intensity occurs. If a linear heating rate, $\beta = dT/dt = \text{constant}$ is used, then the following temperature rate equation exists with

$$-\frac{dh}{dT} = \frac{h K_0}{\beta} e^{-E/kT} \quad (3)$$

Figure 2 illustrates that some of the trapped charge (electrons) near the surface is thermally excited over the surface barrier while simultaneous bulk excitations produce luminescence. This then implies that some of the free charge concentration contributes to the charge emission. If it is assumed that a fraction p ($0 \leq p \leq 1$) of the free charge concentration does contribute to the charge emission, then the rate determining

equation for the charge emission follows:

$$- dc/dT = \frac{c K_o}{\beta} e^{-E/kT} \quad (4)$$

where $c = ph$ is the concentration of untrapped charge contributing to the charge emission.

Two models of activation energy analysis will now be applied to Equation (4). The first and most common model to be applied is the initial-rise method, first advocated by Garlick and Gibson (10). From (4) follows

$$\ln \left(- \frac{dc}{dT} \right) = - E/kT + \ln c(T) + \ln K_o/\beta . \quad (5)$$

The activation energy can then be determined from the slope of the straight line produced by a plot of $\ln(-dc/dT)$ vs. $1/T$ for low temperatures at which the concentration of trapped charge has changed only by negligibly small values. This same idea is also applicable to the charge that contributes to the luminescence. Emphasis is restricted here to the charge emission for clarification.

Braunlich (39) has shown that a rough criterion of the applicability of the initial-rise method is provided by the condition

$$R \cdot h(T_o)/f(T_o) \ll 1 \quad (6)$$

where R is the ratio of the coefficient of the trapping transition δ to the coefficient of the recombination transition γ . $h(T)$ is the concentration of trapped charge at a temperature T much less than the temperature at which the charge emission or glow curve exist, while $f(T)$ repre-

sents the concentration of the unoccupied recombination centers. Figure 2 illustrates δ , γ , $h(T)$ and $f(T)$.

The second model of analysis consists of the Balarin-Zetsche (40) method which utilizes the entire peak under consideration. The integration of (4) is given by

$$- \int_{c_o}^{c(T)} \frac{dc}{c} = \frac{K_o}{\beta} \int_0^T e^{-E/kT} dT. \quad (7)$$

Since the temperature range of interest is such that $T \ll E/k \equiv T_o$, the right side of (7) can be approximated by

$$K_o/\beta \int_0^T e^{-T_o/T} dT \approx \frac{K_o T^2}{\beta T_o} e^{-T_o/T} \{1 - \Sigma\}. \quad (8)$$

where

$$\Sigma = \frac{2T}{T_o} - \frac{6T^2}{T_o^2} + \frac{24T^3}{T_o^3} - + \dots \sum_{\ell=1}^{\infty} (\ell+1)!(-1)^{\ell+1} \left(\frac{T}{T_o}\right)^{\ell} \quad (9)$$

Now (7) becomes

$$C = \frac{C(T)}{C_o} = \exp \left[- \frac{K_o T^2}{\beta T_o} e^{-T_o/T} \right] \{1 - \Sigma\} \quad (10)$$

where C is the fraction of the trap concentration C_o that dissociates in the temperature interval T and $T + dT$. Figure 3 represents a plot of C versus T and $-dc/dT$ versus T for a linear heating rate.

Setting

$$S(T) = \frac{K_o T^2}{\beta T_o} e^{-T_o/T} \quad (11)$$

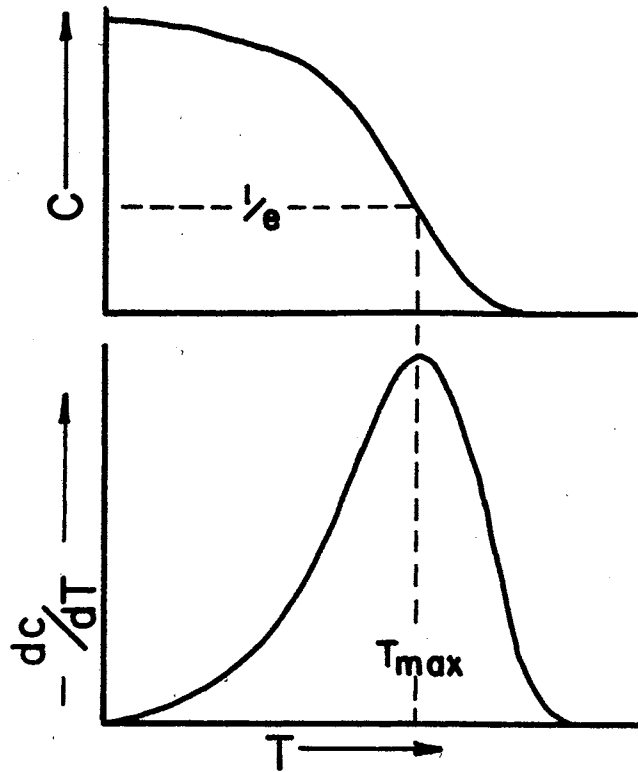


Figure 3. Electron Trap Population C and Its Reduction During Heating

simplifies (10) so that now

$$C = e^{-S} \{1 - \Sigma\} \quad (12)$$

Now from $\left. \frac{d^2C}{dT^2} \right|_{T=T_m} = 0$ it follows that $S(T_m) = 1$ which produces

an expression for the frequency factor of the form

$$K_o = \frac{\beta E e^{E/kT_m}}{kT_m^2} \quad (13)$$

Also from Equation (12) follows

$$\begin{aligned} \ln [-\ln C(T)] &= \ln S + \ln \{1 - \Sigma\} \\ &= -T_o/T + \ln \frac{K_o T_o}{\beta} - 2 \ln T_o/T + \ln \{1 - \Sigma\} . \end{aligned} \quad (14)$$

If Equation (14) is differentiated with respect to $1/T$ an expression will result that determines how accurate this method is for evaluating E if the plot of $\ln [-\ln C(T)]$ versus $1/T$ is considered.

$$\begin{aligned} \frac{d}{d(1/T)} \{\ln [-\ln C(T)]\} &= -T_o + 2T \left[-1 + \frac{T/T_o - 6 T^2/T_o^2 + 36 T^3/T_o^3 - \dots}{1 - \Sigma} \right] \\ &= -T_o + 2T \left[-1 + \frac{\Sigma}{1 - \Sigma} \right] \end{aligned} \quad (15)$$

For a given value of T/T_o , the difference between alternate terms decreases until $(\ell + 1)!$ begins to dominate the series (59). Therefore, Σ represents a cutoff of the series while this difference is small meaning that Σ is a number much less than unity. (15) then becomes

$$\frac{d}{d(1/T)} \{\ln [-\ln C(T)]\} \approx -T_o - 2T \quad (16)$$

This implies that a plot of (14) vs. $1/T$ will yield the activation energy E within the accuracy of $4kT$ where $2kT$ for $500^\circ K = 0.1$ ev.

CHAPTER III

EXPERIMENTAL DETAILS

Introduction

In Chapters I and II it was pointed out that charge emission can be affected by sorption. If the emission is studied with a gas counter then the effects of sorption would be hard to study. It would be necessary to experimentally detect the emission in a high vacuum in order to better understand the effects of gas coverage on the sample surface. This chapter concerns the explanation of two experimental arrangements used and designed in this lab to detect the charge emission in a counting gas atmosphere and in a high vacuum. The technique of simultaneously detecting the T.S.L. will also be briefly explained. This is then followed by a brief explanation of the E.S.R. equipment used, sample preparation and materials other than MgO that have been examined with the gas counting apparatus.

Apparatus and Measuring Techniques

Gas Counting

Figure 4 represents a block diagram of the gas counting equipment, while Figure 5 illustrates the main part of the Geiger tube type gas flow counter. The system is evacuated and then pressurized to 7 cm. of Hg with a 90% Argon and 10% Methane counting gas. The pressure of the

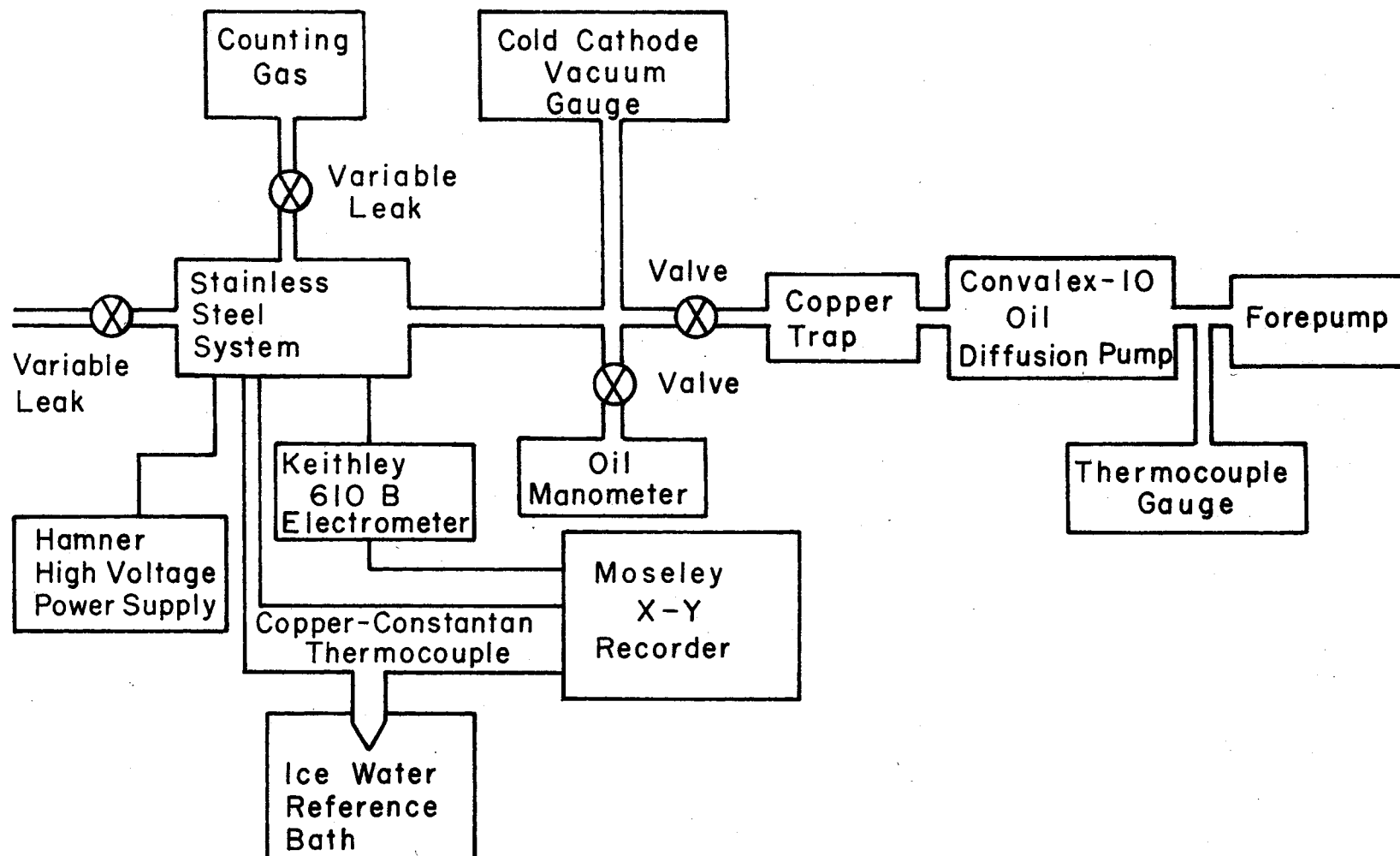


Figure 4. Block Diagram of Gas Counting Equipment

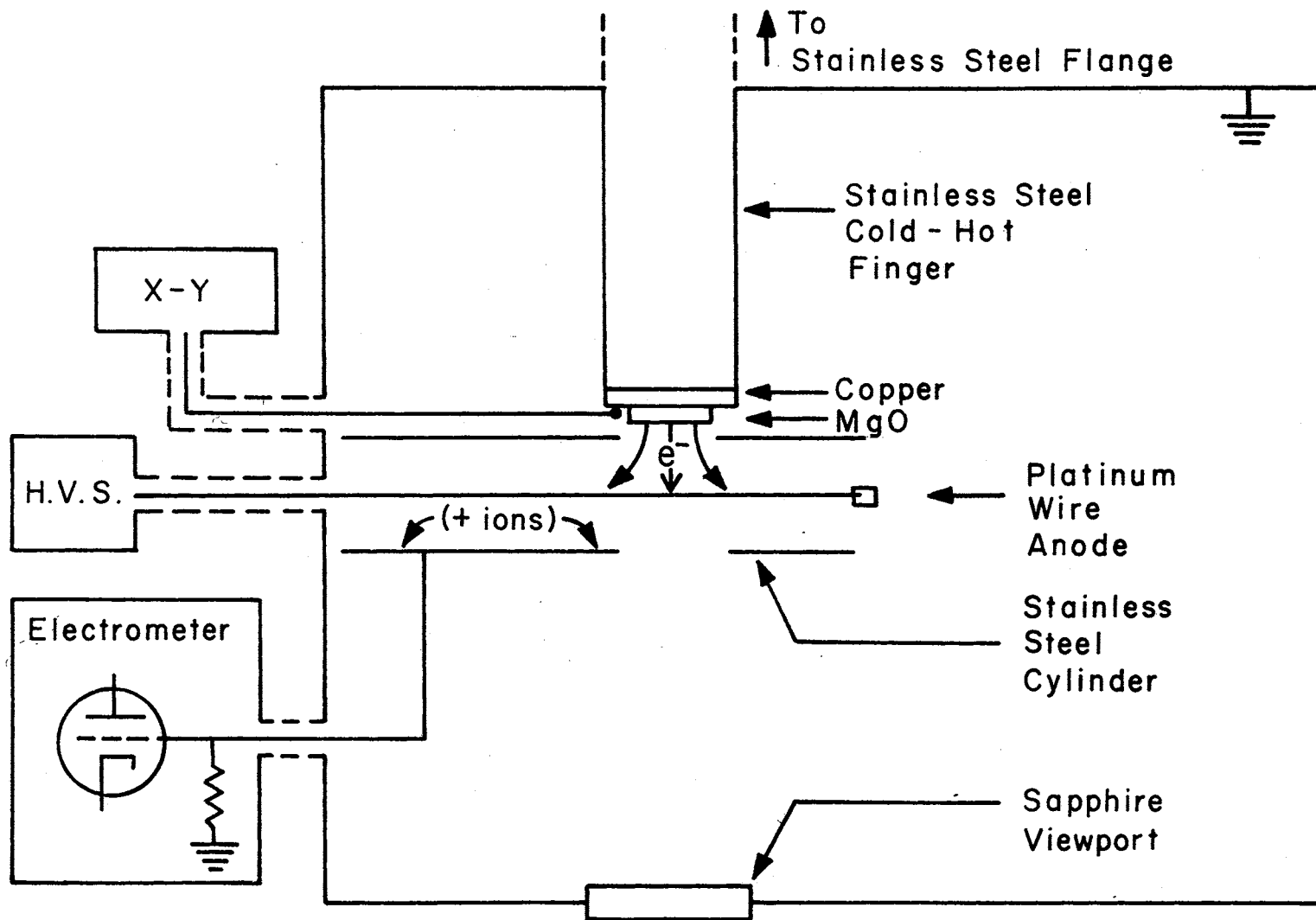


Figure 5. T.S.C.E. Gas Detection System

counting gas is monitored with a low vapor pressure oil (n - butyl phthalate) both before and after recording the charge emission. The gas flow through the detector is controlled by an Edwards high vacuum variable leak at the input of the counting gas to the sample chamber, and a Granville-Phillips series 204 Gold seal ultra-high vacuum valve, at the output of the gas flow from the chamber, such that the pressure measured at room temperature before and after a characteristic experiment is within ± 0.50 cm on the average. The sample is lowered to near 77°K after pressure stabilization at 7 cm. of Hg near 295°K . Then excitation follows through the sapphire viewport with the full band of ultraviolet light from a 100 watt Hanovia Hg lamp and subsequent linear heating to 600°K . Characteristic heating rates of 0.35°K/sec and 0.56°K/sec were used below and above room temperature respectively. Subsequent heating of the MgO , then, produces charge emission and luminescence at characteristic temperatures, with the charge emission producing ions and electrons in the counting gas. This ionization of the counting gas is produced by the acceleration of the charge emitted from the MgO by the electric field produced by the anode voltage (+ 1000 volts). Electrons from the ionization are attracted to the anode while the ions are neutralized at the stainless steel cylinder. The stainless steel cylinder is attached to earth ground through the resistance of a Keithley 610B electrometer, which allows for the detection of the charge emission. Currents as small as 10^{-14} ampere can readily be detected with this arrangement. Characteristic T.S.L. measurements are made with a voltage divider arrangement with the cathode of the 1P28 photomultiplier at -1100 volts and the collector at earth ground. The T.S.L. current is monitored with another electrometer. The outputs of the electrometers are then fed

into two separate x-y recorders, with the T.S.C.E. and the T.S.L. currents being recorded simultaneously, versus the temperature of the surface of the sample.

Korff (41) has an excellent book about electron and nuclear counters, where all of the characteristics of counters are explained and discussed in detail. As Korff points out a specific gas amplification factor exists for each type of counting gas used. This factor depends primarily on the geometry of the counter, the voltage applied to the anode, the shape and diameter of the anode and the pressure of the counting gas. When the accelerated charge from MgO produces free electrons in the gas, these electrons are swept toward the center wire where they eventually gain sufficient kinetic energy to cause additional gas ionization. This electron multiplication process, therefore, produces at the anode, an electrical charge many times greater than that caused by the initial ionizing event. A quantitative measure of this electron multiplication is the gas amplification factor, which is the average number of electrons reaching the anode per electron liberated in the initial ionizing event. Diethorn (42) has developed an equation for the amplification factor for a counter used in the proportional region, while Kiser (43), Kiser and Storrs (44), have shown that Diethorn's equation not only holds for counters used in the proportional region, but also in the Geiger region of operation for various gas pressures, anode voltages and radii. Diethorn's equation follows:

$$\ln A_o = \frac{0.7 V}{\Delta V \ln (b/a)} \ln \left[\frac{V}{K p a \ln (b/a)} \right] \quad (17)$$

where

V = potential difference between the anode and cylinder wall,

a = radius of anode platinum wire,

b = radius of cylinder,

p = gas pressure in counter,

$\overline{\Delta V}$ = average potential difference through which the electron moves in covering some distance d , and

\overline{K} = E_0/p , with E_0 representing the electric field intensity below which no ionization occurs.

Values for $\overline{\Delta V}$ (30 volts) and \overline{K} (100 V/in. mm. Hg) were obtained from Kiser's report for a gas consisting of 7.9% CH_4 and 92.1% Ar. Substituting $\overline{\Delta V}$ and \overline{K} into (17) gives a value of $A_0 = 1.4 \times 10^4$. According to Korff (41), this value for the multiplication factor implies that the counter is being operated in the proportional counter region. This also agrees with a plot of the intensity versus the anode voltage, which produces plateaus characteristic of the proportional counting region.

High Vacuum Counting

Figure 6 is a block diagram of the high vacuum emission detecting system, while Figure 7 illustrates the details of the charge detection and its associated electronics. The basic difference in the charge detection is that once the charge is thermally excited from the MgO, it is accelerated by the electric field of the grid toward the cone of the Spiraltron electron multiplier. Subsequent collision with the inside surface of the cone produces secondary electron emissions within the cone of the detector. These secondary emissions are then caught in the axial electric field placed on the Spiraltron by the external high voltage supply. These electrons are then accelerated toward the collector with

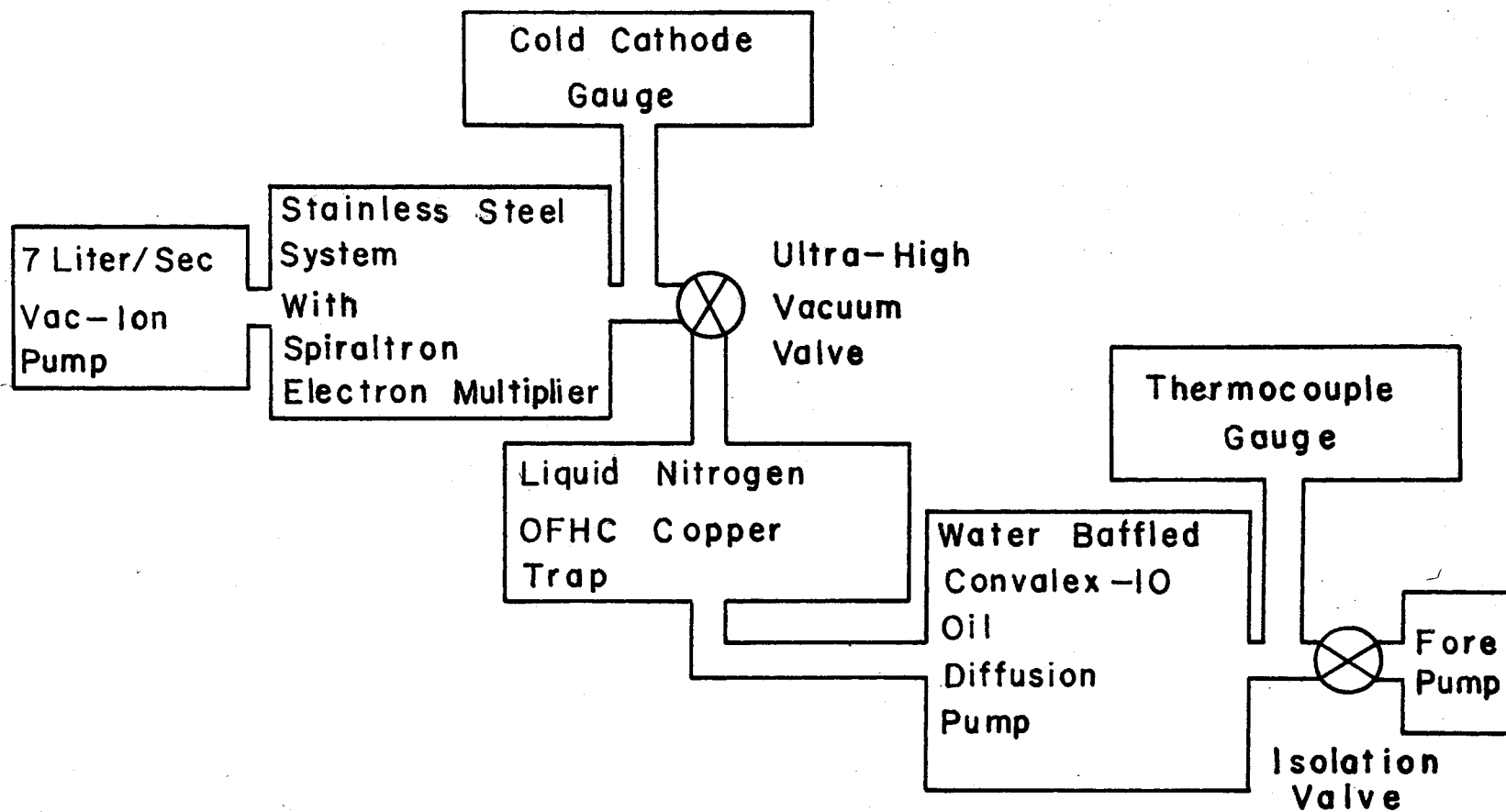


Figure 6. Block Diagram of the High Vacuum Detection System

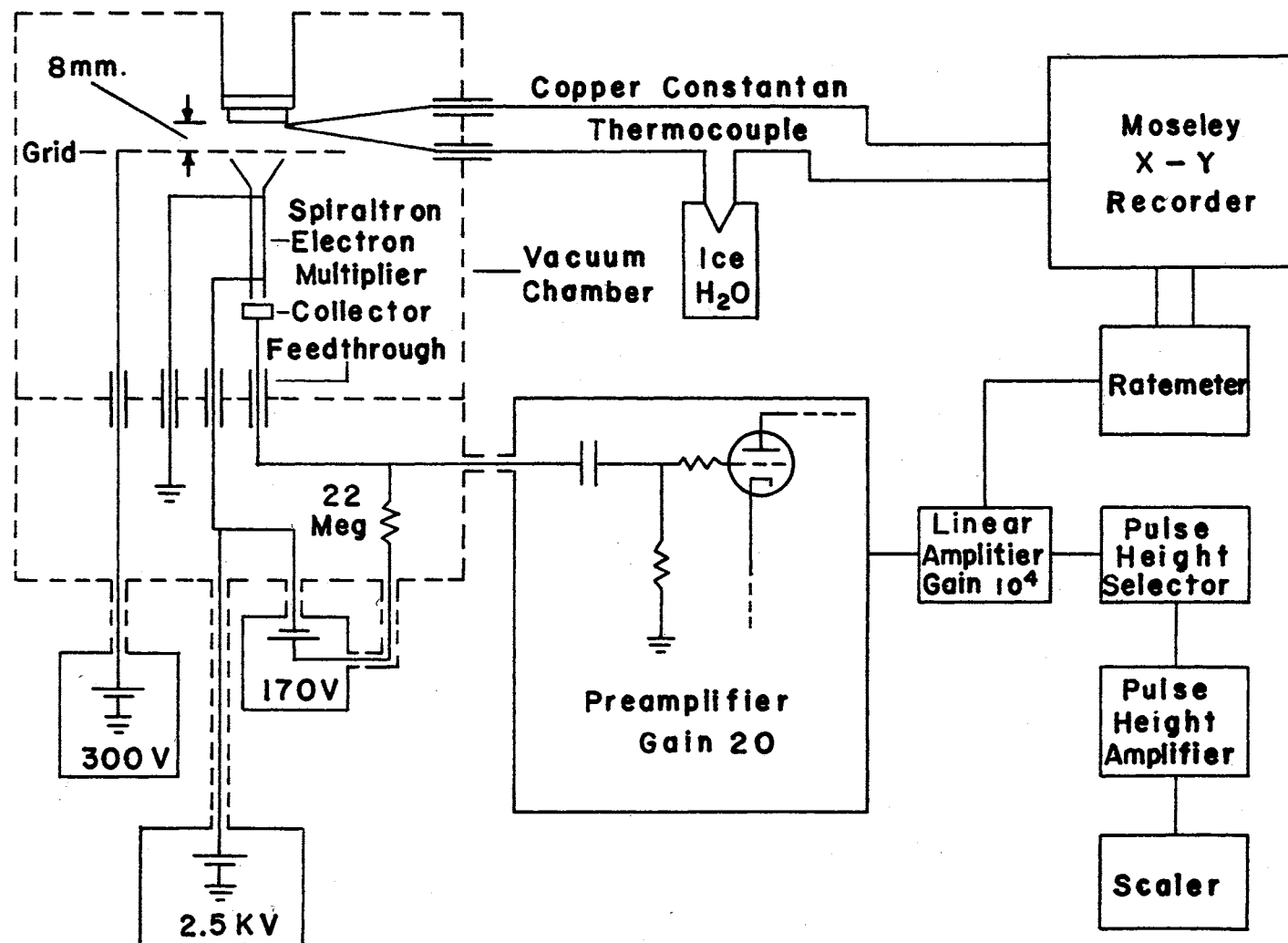


Figure 7. Charge Detector and Associated Electronics

more secondary emissions occurring for each collision of an electron with the inside surface of the electron multiplier. These electrons then arrive at the collector milliseconds after the first secondary emission in the cone occurs. For each charge producing a secondary emission at the cone, there will be from 10^7 to 10^8 electrons arriving at the collector. These pulses of current then produce voltage drops across the 22 megaohm resistor that are accepted by the preamplifier, and then further amplified by the linear amplifiers to be recorded as a count rate from the output of the ratemeter. This count rate is then recorded on the y-axis as a function of the temperature of the sample surface.

Electron Spin Resonance Spectrometer

The E.S.R. spectrometer was of the homodyne reflection type with 16 KHz magnetic field modulation. A Varian V-4531 cavity was used, which had horizontal slots in one side to permit the excitation of the sample with light in the cavity. The sensitivity of the system allowed detection of approximately 2×10^{12} spins at 77°K . Operation near 125°K and above to 525°K was possible by flowing nitrogen gas through stainless steel tubing submerged in liquid nitrogen, or through a variable temperature control heating element for the low and high temperatures respectively. The temperature of the sample was determined with a thermocouple near the sample. With this gas flow system, temperature in the cavity could be controlled to within 5°K , or varied, allowing temperature runs similar to the luminescence or charge emission.

Observation of Materials Different From MgO

A variety of materials consisting of $\text{SnP}_2\text{:Zn}$, KMgF_3 , and Al_2O_3

(sapphire) were initially studied in conjunction with MgO. All of the above materials produced charge emission except $\text{SnO}_2\text{:Zn}$. A more thorough study would have to be performed on this material before detailed comment could be presented. Charge emission occurred from KMgF_3 without corresponding luminescence (1P28 photomultiplier) when the sample was irradiated with ultraviolet light. However, when gamma irradiated, intense luminescence appeared in addition to charge emission both below and above room temperature. This was indicative of more radiation damage being produced by the gamma excitation, while Al_2O_3 produced both luminescence and charge emission as a result of ultraviolet excitation.

With respect to all of the materials investigated, it was obvious that the charge emission and luminescence from MgO were more consistent and reproducible. Since more information was readily available (e.g., color centers, radiation damage, optical absorption) for this material, it was decided that a further study would be more beneficial for answering some of the questions concerning charge emission and exploring MgO in this respect, for a literature search indicated that no detailed information concerning the nature of charge emission from this material was available.

MgO Samples and Their Preparation

The samples were nominally pure containing up to 10 p.p.m. of Fe, Cr, Mn and up to 50 p.p.m. of other impurities (i.e., Si, Al, Ca, etc.). They were cleaved into a parallelepiped geometry such that the (100) face could be exposed to the charge and luminescence detectors. A variety of sizes were observed having surface areas ranging from 0.3 cm^2 to 1 cm^2 and thicknesses from less than 1 mm. to 2 mm. The samples were

always chemically polished (68) in 85% H_3PO_4 acid at a temperature of 333°K for an average of 20 minutes, rinsed thoroughly in distilled H_2O and then briefly washed with reagent grade acetone. After the chemical polish the crystals were placed immediately into the system with care such that no contamination from the environment was allowed.

CHAPTER IV

EXPERIMENTAL RESULTS

Introduction

In order to (1) establish a model for T.S.L., (2) determine the nature of the charge emission, (3) present a qualitative idea of the energy with which the charge is emitted and, (4) correlate data to better understand the mechanism of T.S.C.E. from MgO, the following presentation of experimental results will be given.

Characteristic T.S.L. and T.S.C.E. Measurements

Experimental results obtained from a variety of crystals after ultraviolet irradiation are presented first.

Emission Spectroscopy

The wavelength distribution of the T.S.L. from a characteristic crystal is reported in this section and compared with filtered T.S.L.

Electron Spin Resonance

Characteristic spectra are presented here and the results compared with the emission spectroscopy.

T.S.L. Using a Blue and Red Sensitive Photomultiplier

Experimental results using an RCA-7102 photomultiplier tube are

presented here.

Gamma Irradiation Effects

T.S.L. and T.S.C.E. measurements from a variety of crystals are discussed in this section after the crystals were irradiated with gamma rays or gamma rays and the full band of ultraviolet light.

Bleaching Effects on T.S.L. and T.S.C.E.

Experimental results are presented here that indicate the effect of different bleaching wavelengths on T.S.C.E. and T.S.L. after excitation with ultraviolet light. Bleaching with filtered ultraviolet light after gamma irradiation is also discussed.

T.S.C.E. Peak Intensity Changes

Peak intensity changes in the gas system as well as in the high vacuum system are presented here.

Magnetic Field and Grid Voltage Effects on T.S.C.E.

The results of observing the charge emission with and without an external magnetic field and also comments concerning the effect on T.S.C.E. by changing the grid voltage are presented.

Characteristic T.S.L. and T.S.C.E. Measurements

The experimental results shown in Figures 8, 9 and 10 were obtained in the gas system after the samples had been excited near 77°K with the full band of ultraviolet light and subsequently heated to near 260°K , cooled back below 236°K and again heated to 700°K . The heating rates

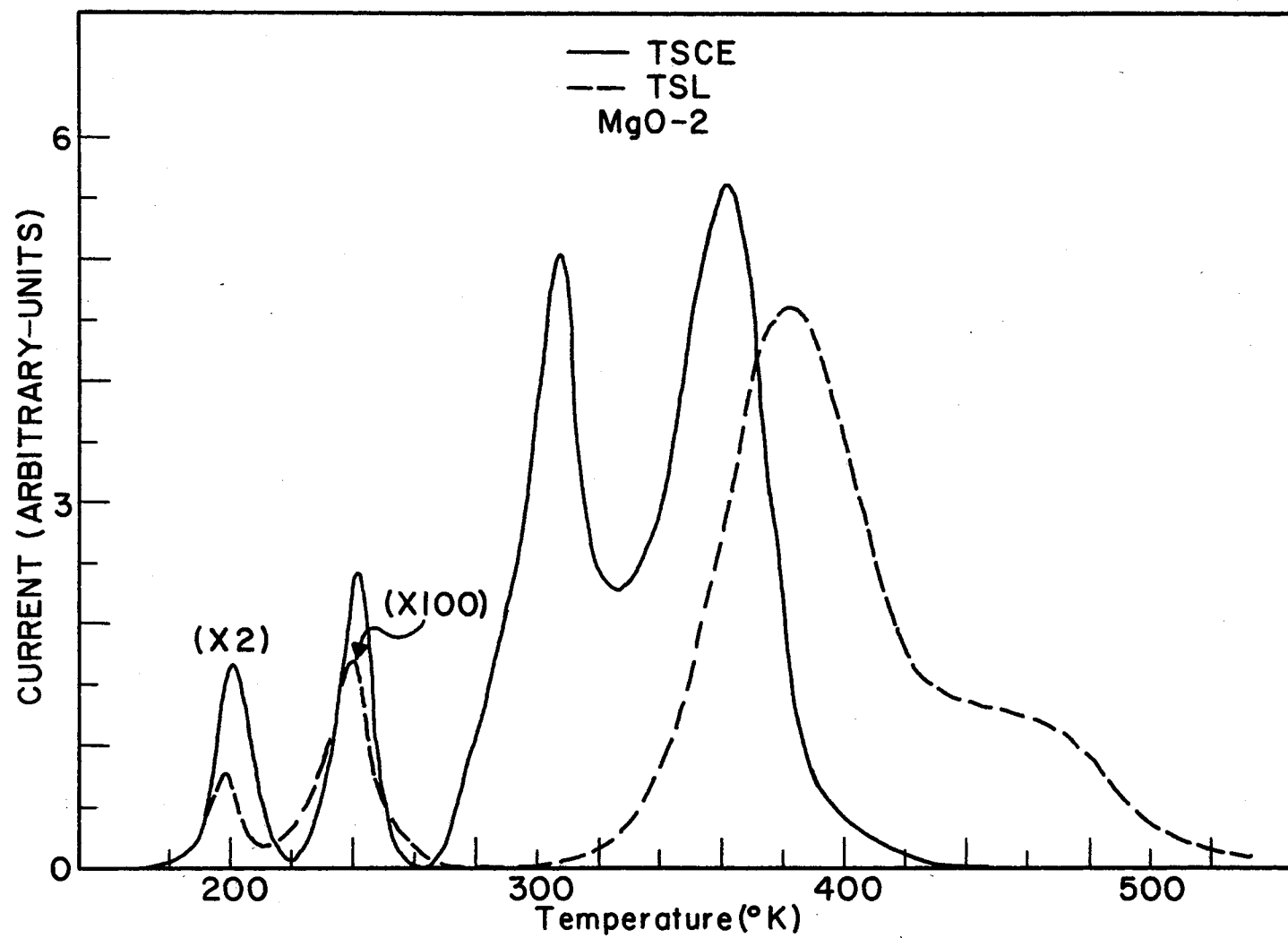


Figure 8. T.S.C.E. and T.S.L. From MgO-2

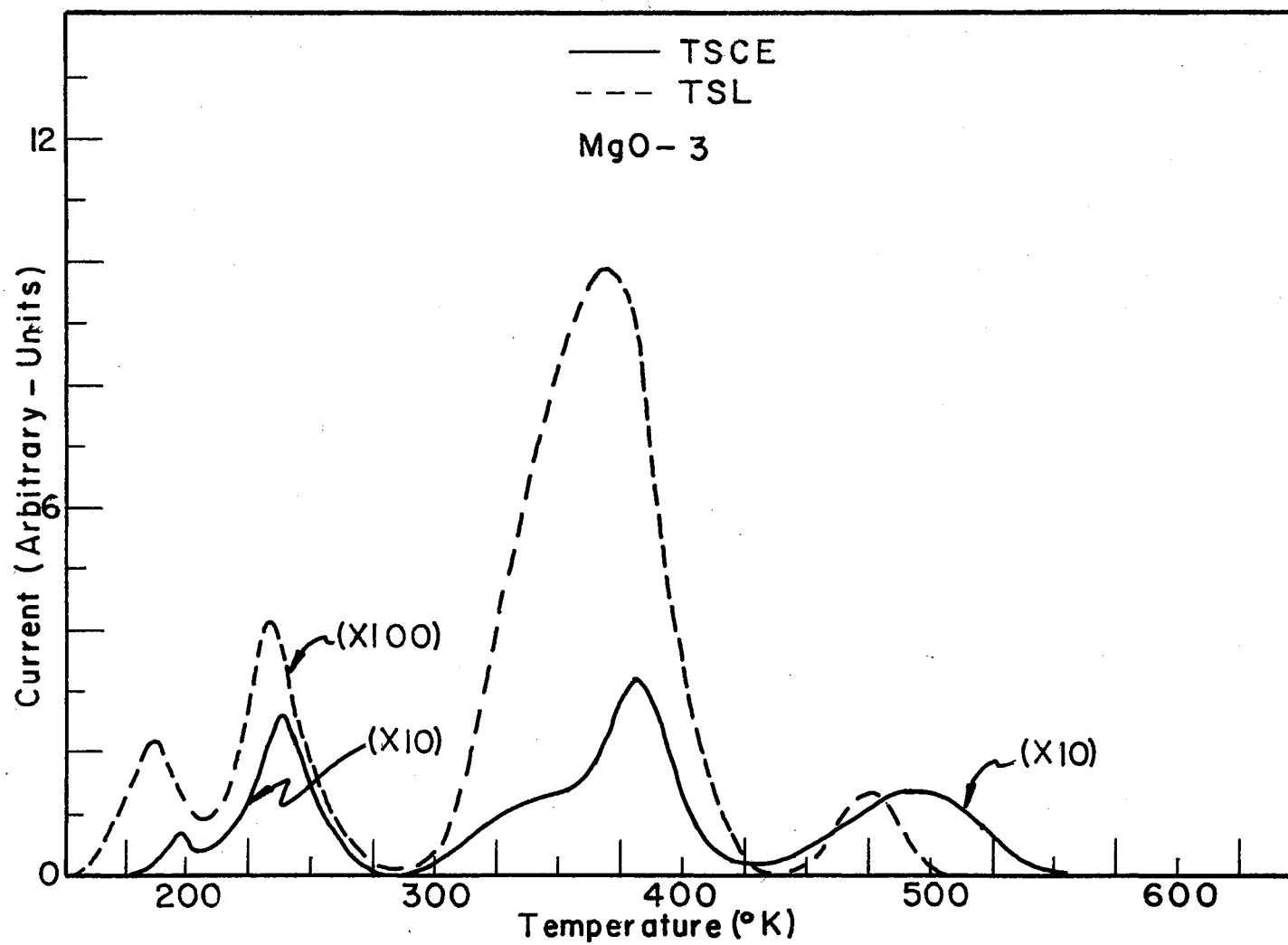


Figure 9. T.S.C.E. and T.S.L. From MgO-3

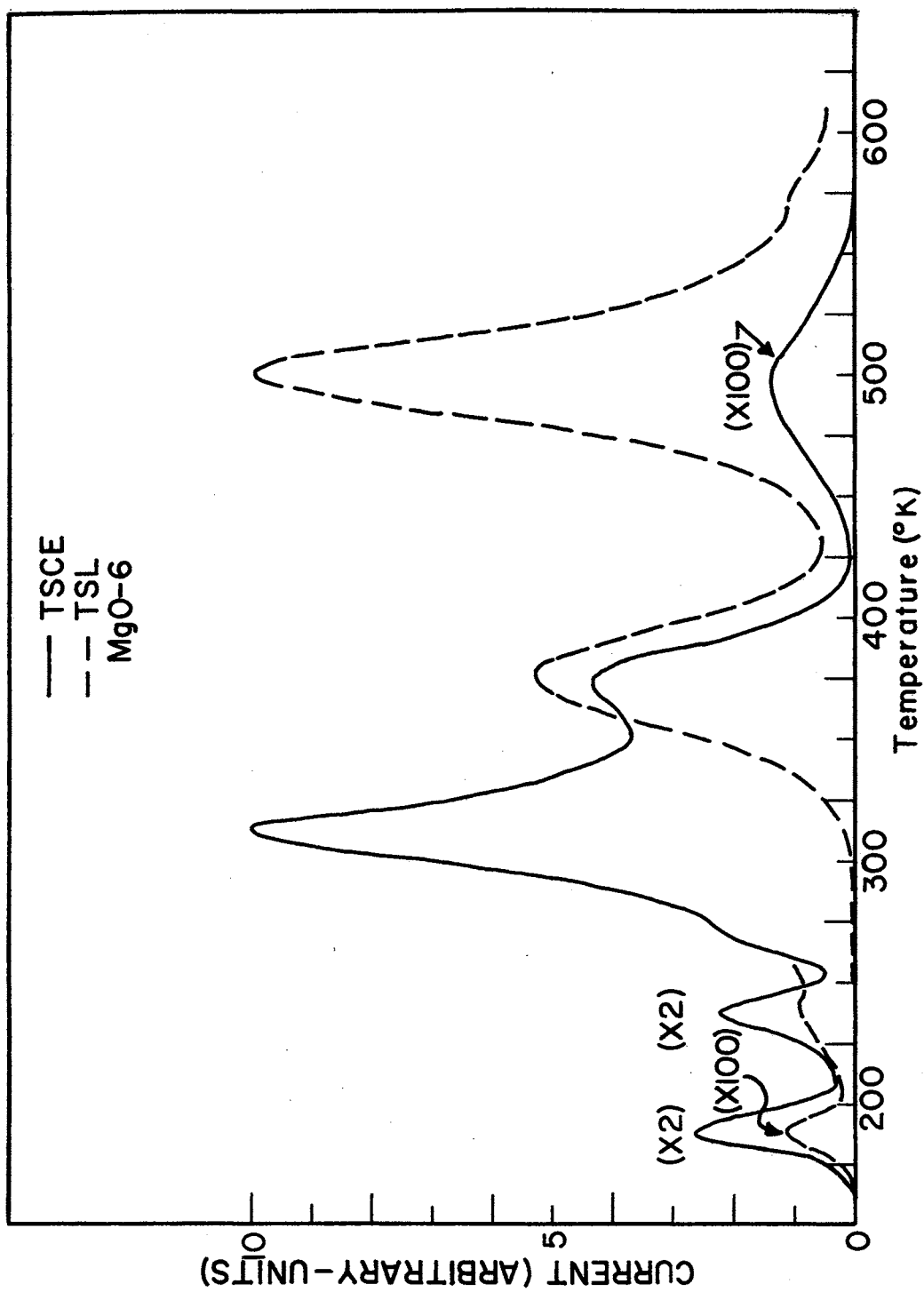


Figure 10. T.S.C.E. and T.S.L. From MgO-6

were $0.35^{\circ}\text{K}/\text{second}$ and $0.55^{\circ}\text{K}/\text{second}$ below and above room temperature respectively. After the 1000 seconds of irradiation, 1000 seconds delay was used before heating the samples. This delay allowed the electrometers to reach a good high sensitivity equilibrium and for any possible afterglow to subside below a detectable level. The 1000 seconds of irradiation does not saturate the traps in the crystals but was chosen because it yielded measurable charge emission as well as luminescence and also helped minimize the time between consecutive runs. As the figures indicate the low temperature T.S.L. peaks are of very low intensity. Here all of the luminescence was recorded with an RCA-1P28 photomultiplier which is more sensitive to blue light. Table I presents the characteristic peak positions with respect to temperature and their intensities.

Emission Spectroscopy

Figure 11 represents the spectral distribution of MgO-6. The sample was taken after an annealing temperature of 600°K and irradiated for 30 minutes at room temperature with the full band of the Hg lamp. It was then heated to 600°K with the light emission being passed through a monochromator. The 300 to 500 nanometer scan was started using the blue sensitive 9558 photomultiplier tube in the temperature range from $(T_{\text{Max.}} \pm 25)^{\circ}\text{K}$ for the 383°K and the 500°K T.S.L. peaks respectively. The sample was then irradiated again at room temperature and a repeat scan was made this time using a blue to predominantly red 7102 photomultiplier tube from (550 to 750) nanometers. The scale on the left side of Figure 11 refers to the (300 to 500) nanometer scan while that on the right refers to the (550 to 750) nanometer scan. As indicated

TABLE I

INFORMATION PERTAINING TO THE GLOW AND CHARGE EMISSION CURVES OF FIGURES 8, 9 AND 10

Sample	Temperature ($T_{\text{Max.}}$ -°K) of the T.S.L. Peak Maximum	Temperature ($T_{\text{Max.}}$ -°K) of the T.S.C.E. Peak Maximum	Peak PMT Current (10^{-11} amps.)	Peak T.S.C.E. Current (10^{-11} amps.)
MgO-2	200	203	0.01	0.18
	239	242	0.02	0.53
		307		1.1
		363		
	383		6	1.2
	466		1.7	
MgO-3	188	197	0.036	0.01
	235	240	0.063	0.07
		323		0.20
	377		15	
		385		0.70
	475		1.8	
MgO-6		508		0.50
	189	180	0.015	0.276
	236	236	0.01	0.237
		311		2.19
	383	375	7	0.945
	500	500	13.2	0.03

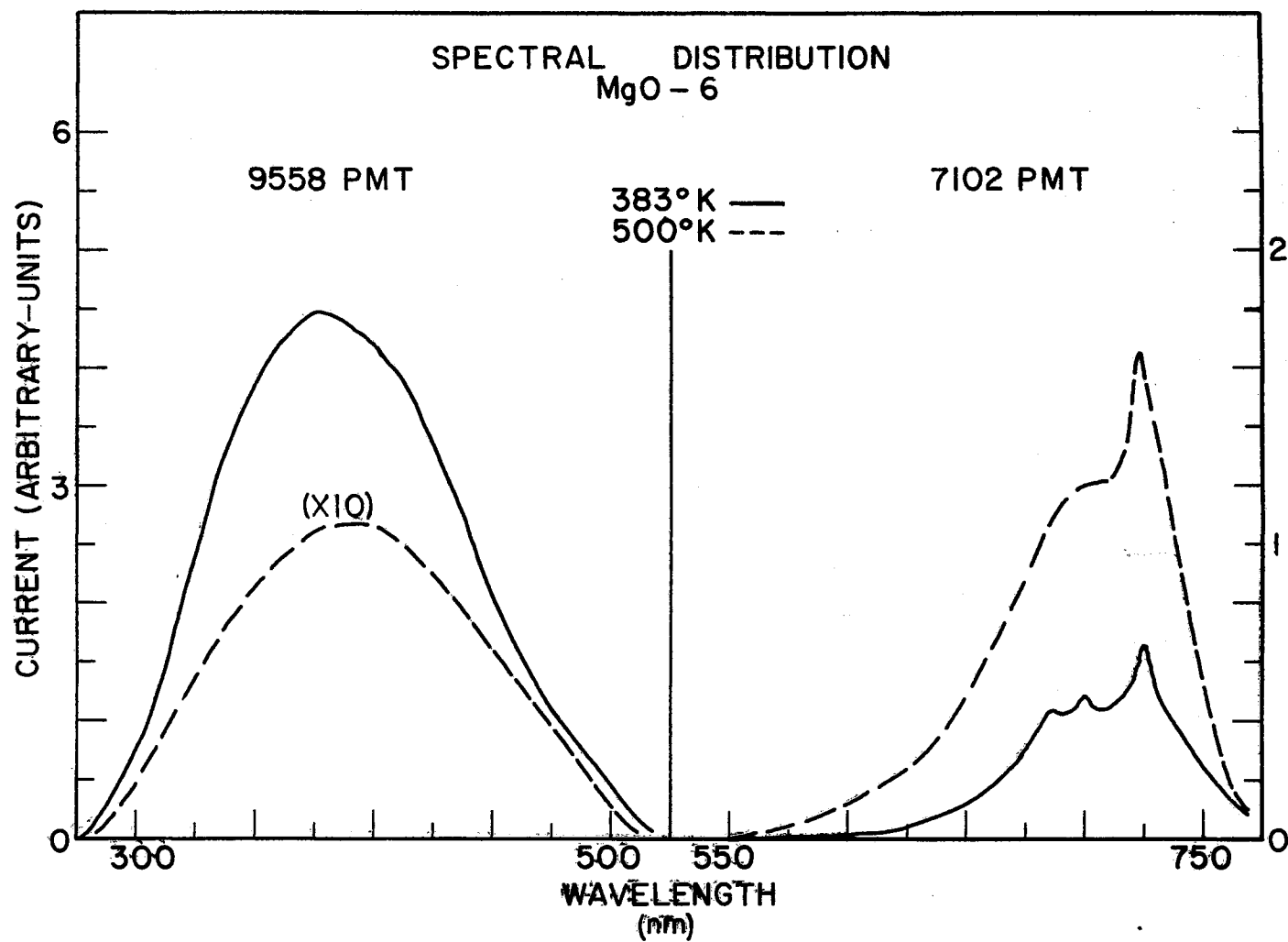


Figure 11. Spectral Distribution of MgO-6

the 383°K peak consists mainly of blue luminescence, while the reverse is true for the 500°K peak.

Figure 9 shows that the 377°K T.S.L. peak of MgO-3 is approximately 8 times more intense than the 475°K peak. When the luminescence is observed through a 550 nanometer filter the 475°K peak has more intensity implying that more red luminescence is occurring with the 475°K peak while the 377°K peak is more in the blue. A similar check with a 440 nanometer filter yields a 377°K peak that is 3.5 times as intense as the 475°K. The results seem to compare favorably with the emission data of MgO-6.

E.S.R. Spectrometer

Figure 12 represents the electron spin resonance runs from MgO-6 and is comparatively characteristic of MgO-2 and MgO-3. Here the sample was annealed to 600°K and then the "No Irradiation" run made at room temperature. Following this, the sample was irradiated with the full ultraviolet light band as indicated and then the electron spin resonance performed. This then shows the Mn^{2+} increasing with the Fe^{3+} and Cr^{3+} decreasing. The V^- center also increased here but because of line broadening it does not appear above room temperature. It was, however, verified in a 140°K temperature scan. The sample was then heated to 393°K for 5 minutes and after cooling to room temperature the spectrum was again recorded. This run shows Mn^{2+} the same, while Fe^{3+} and Cr^{3+} have increased. The Fe^{3+} increase is the most obvious. The V^- center is completely gone at this point which again had to be verified near 140°K.

The sample was then heated to 523°K for 7 minutes and cooled back

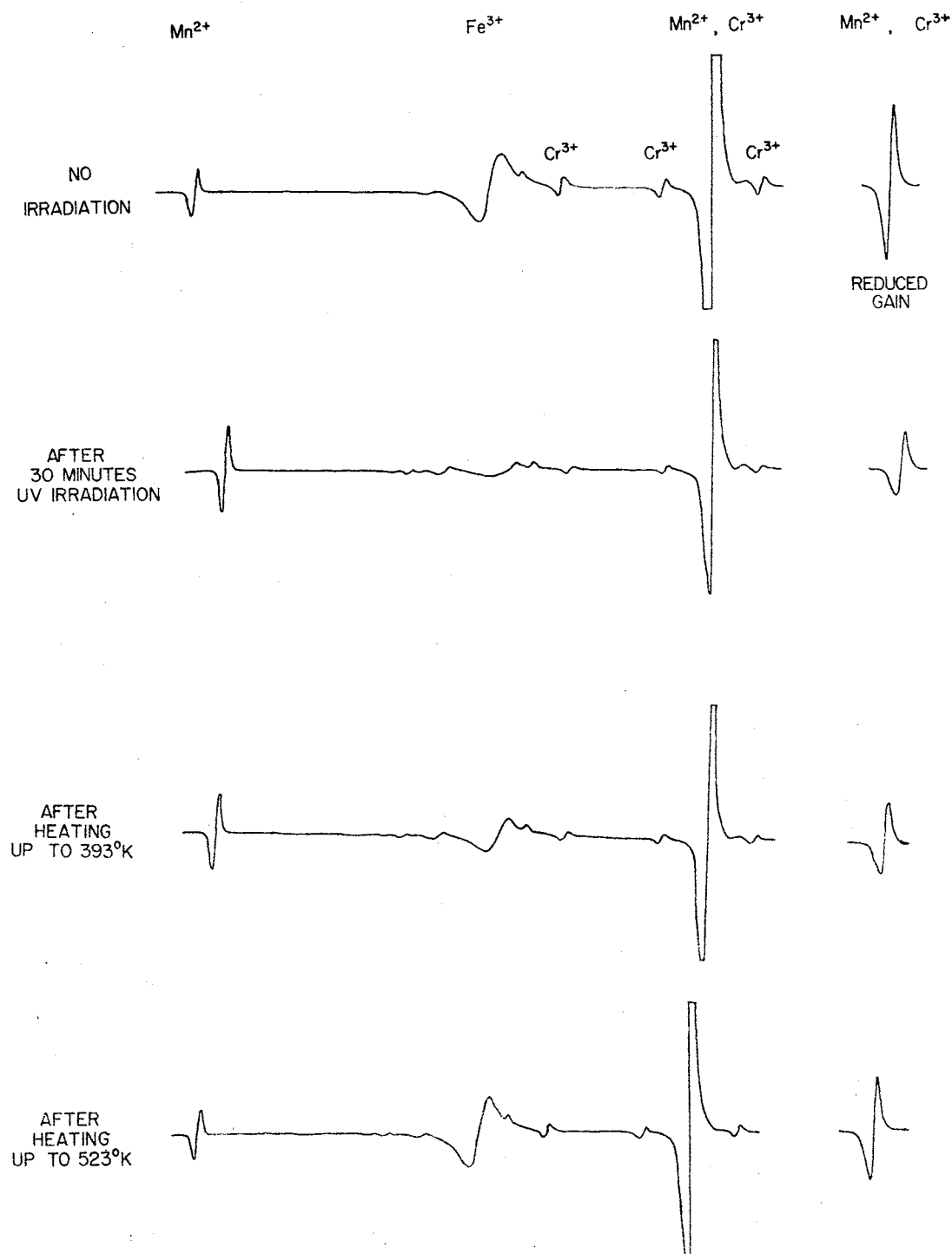


Figure 12. E.S.R. From MgO-6

to room temperature with a subsequent spectrum indicating that the Mn^{2+} is now back to normal, while Fe^{3+} and Cr^{3+} have again increased.

Table II summarizes the E.S.R. spectra and compares the results with the emission spectroscopy.

TABLE II
SUMMARY OF E.S.R., T.S.L., T.S.C.E. AND
EMISSION SPECTROSCOPY FROM MgO-6

Observations	383°K Peak	500°K Peak
Different Centers Involved	V^- Decreases Fe^{3+} and Cr^{3+} Increase	Mn^{2+} Decreases Cr^{3+} and Fe^{3+} Increase
Spectral Distribution of TSL	Blue, Red	Red, Blue
Charge Emission	Strong Emission	Weak Emission

T.S.L. Using a Red and Blue Sensitive Photomultiplier

Table I shows charge emission peaks in the vicinity of 310°K while there seems to be no corresponding T.S.L. in this region. Figure 13 represents a glow curve from MgO-2 using an RCA-7102 photomultiplier. This tube has a narrow blue sensitive region from (300-400) nanometers and a larger red sensitive region from (450-1100) nanometers, being approximately twice as sensitive in the blue region. The results indicate the 309°K peak that was not observable with the (200-650) nanometer sensitive 1P28 photomultiplier. Since both tubes peak in sensitivity near the middle of the regions listed, it is obvious that the 309°K peak luminescence occurs someplace above 650 nanometers. That the low tempera-

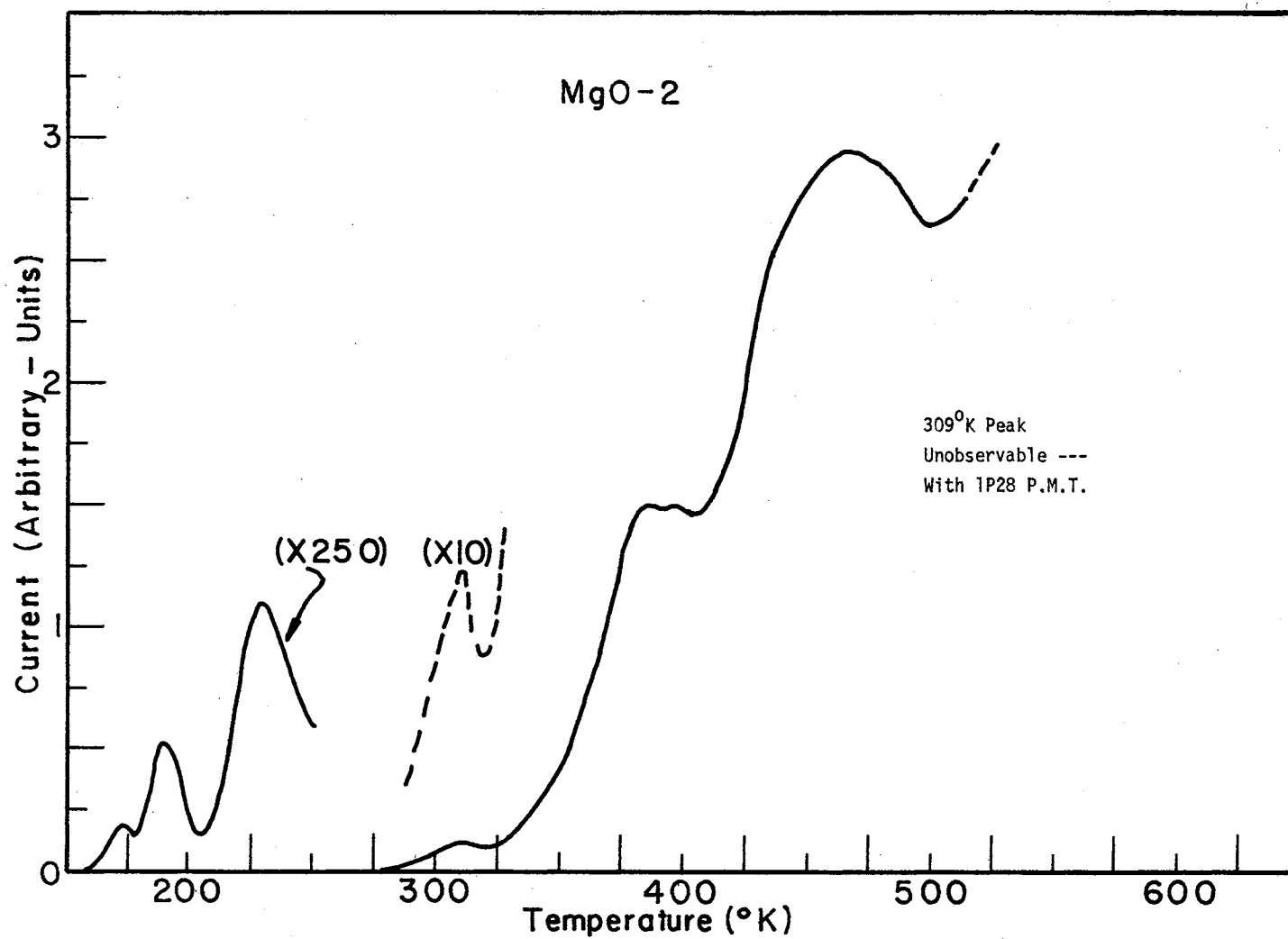


Figure 13. T.S.L. From MgO-2 With an RCA-7102 Photomultiplier

ture peaks are observable with both tubes and that they have similar intensities would imply luminescence in the blue region. Although the glow curve was not corrected for background glow as the well became hot, it was noticed that the contribution did not become significant until a temperature near 410°K . The two peak structures near 384°K and 397°K imply that there is blue and red emission in this temperature region. Structure near 441°K and 470°K is also observable.

Gamma Irradiation Effects

A variety of MgO samples including MgO-2, MgO-3, and MgO-6 were subjected on separate occasions to gamma irradiation (1.5 hours at 1700 rads/minute) at 300°K , with the samples being kept in the dark during transfer back to the gas detecting system. Semi-darkness was obtained in the lab during sample mounting. The basic effect on the T.S.L. (1P28 observation) was the enhancement of the primary peaks (383 , 377 , 383) $^{\circ}\text{K}$ intensities by an average of 100. As expected, no corresponding luminescence occurred below room temperature. It was also observed that the temperatures of the primary peak maxima shifted on the average 20°K to a lower temperature. The major enhancement of the primary peaks was associated with the increased concentration of V^- centers produced as a result of the higher energy gamma rays, which was verified with electron spin resonance, while the decrease in temperature of the primary peaks near 380°K agrees with other published results concerning MgO which has been irradiated with heavy gamma or X-ray doses (30, 33). It is possible that more re-trapping (small V^- concentration) causes a delayed luminescence, while a less significant re-trapping (large V^- concentration) produces a more rapid appearance of T.S.L. with respect to temper-

ature (12).

Figure 14 represents luminescence that is characteristic of MgO, if the above mentioned gamma irradiation is followed by 5 minutes of excitation with the full band of ultraviolet light near 77°K .

The peak near 188°K is enhanced more than the peak near 235°K , while there is no apparent shift in peak positions with respect to temperature. The double irradiation curve (dashed) implies that the ultraviolet excitation seems to have access to a more heavily populated deep trap which then allows for the production of a larger concentration of filled traps stable only below 188°K (shallow traps). The thermal decay of this larger concentration of shallow traps then produces more luminescence. The more heavily populated deep trap is a consequence of the γ -irradiation, which because of its energy, is capable of populating from an even deeper trap, the trap accessible to the ultraviolet light.

If the ultraviolet excitation was extended beyond 5 minutes, the low temperature luminescence enhancement decreased, while excitations of 35 minutes, and more, decreased the primary peak near 380°K by a factor of 3. The decrease of the primary peak was established by electron spin resonance to be associated with the bleaching of the V^{-} centers.

The charge emission is not affected appreciably by gamma and 5 minute ultraviolet light excitations. The primary peak near 375°K was usually increased by an average factor of 4 and did seem to shift by approximately 5°K toward a lower temperature. The other peaks remained relatively stationary with respect to intensity and temperature.

Bleaching Effects on T.S.L. and T.S.C.E.

The experimental data presented in this section were obtained using

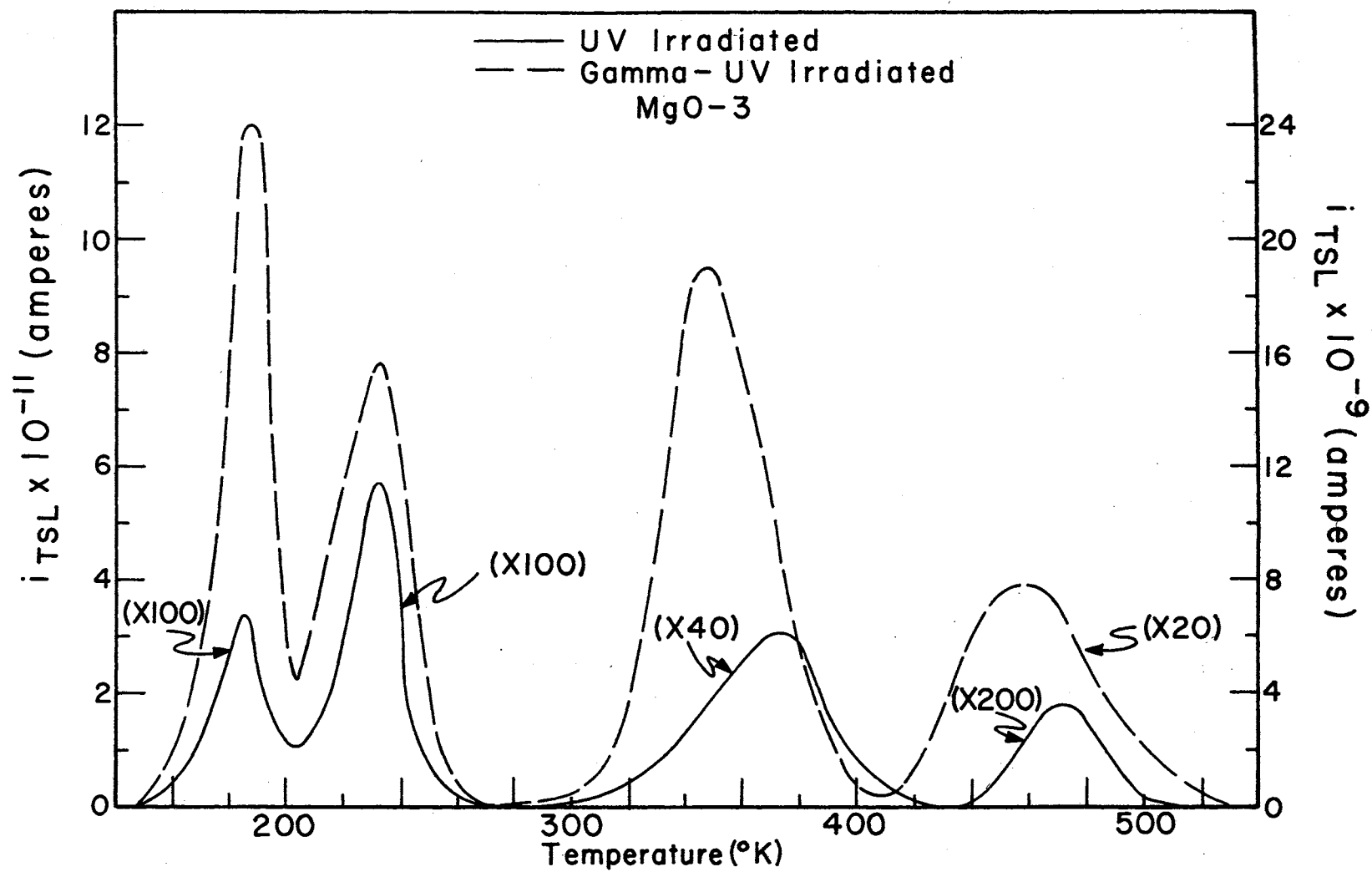


Figure 14. T.S.L. From MgO-3 After Gamma Irradiation at 300°K and Ultraviolet Excitation Near 77°K

the high vacuum system. Initial runs after pumping down to 10^{-8} Torr implied that charge from the vac-ion pump region was producing a higher intensity charge emission peak near 440°K by electron and/or ion bombardment from the pump itself. In order to alleviate this problem the vac-ion pump was turned off when the system was in the 10^{-8} Torr region and then the sample heated to 700°K with the grid voltage at + 300 volts. This removed all of the excess charge peaks from the sample surface as indicated by additional runs with the vac-ion pump off. The pressure of the vacuum system would increase from (10^{-8} to 10^{-6}) Torr as a result of several runs with the vac-ion pump off. This insured then the removal of vac-ion pump effects and also allowed for the safe operation of the 4219X electron multiplier. All of the data to be discussed below were taken after the removal of the excess charge peaks and with the vac-ion pump turned off.

Figure 15 represents the effect on T.S.C.E. of following a 17 minute full band ultraviolet excitation at 300°K by 2 hours of focused 546 nanometer light (also at room temperature). The solid curve is the baseline run (ultraviolet only), while the dashed curve corresponds to the bleaching effect. After the bleach run, the baseline was again reproduced yielding the same solid curve. This then shows that 546 nanometer light will bleach the charge emission peak near 388°K . These runs were made after the sample had been taken through a variety of runs such that the charge emission peak intensities were relatively stable. The primary luminescence peak near 380°K also decreased in intensity but not as much as the charge emission.

The predominant peak near 440°K is produced by the ultraviolet light and as indicated there is no appreciable effect of the bleaching on this

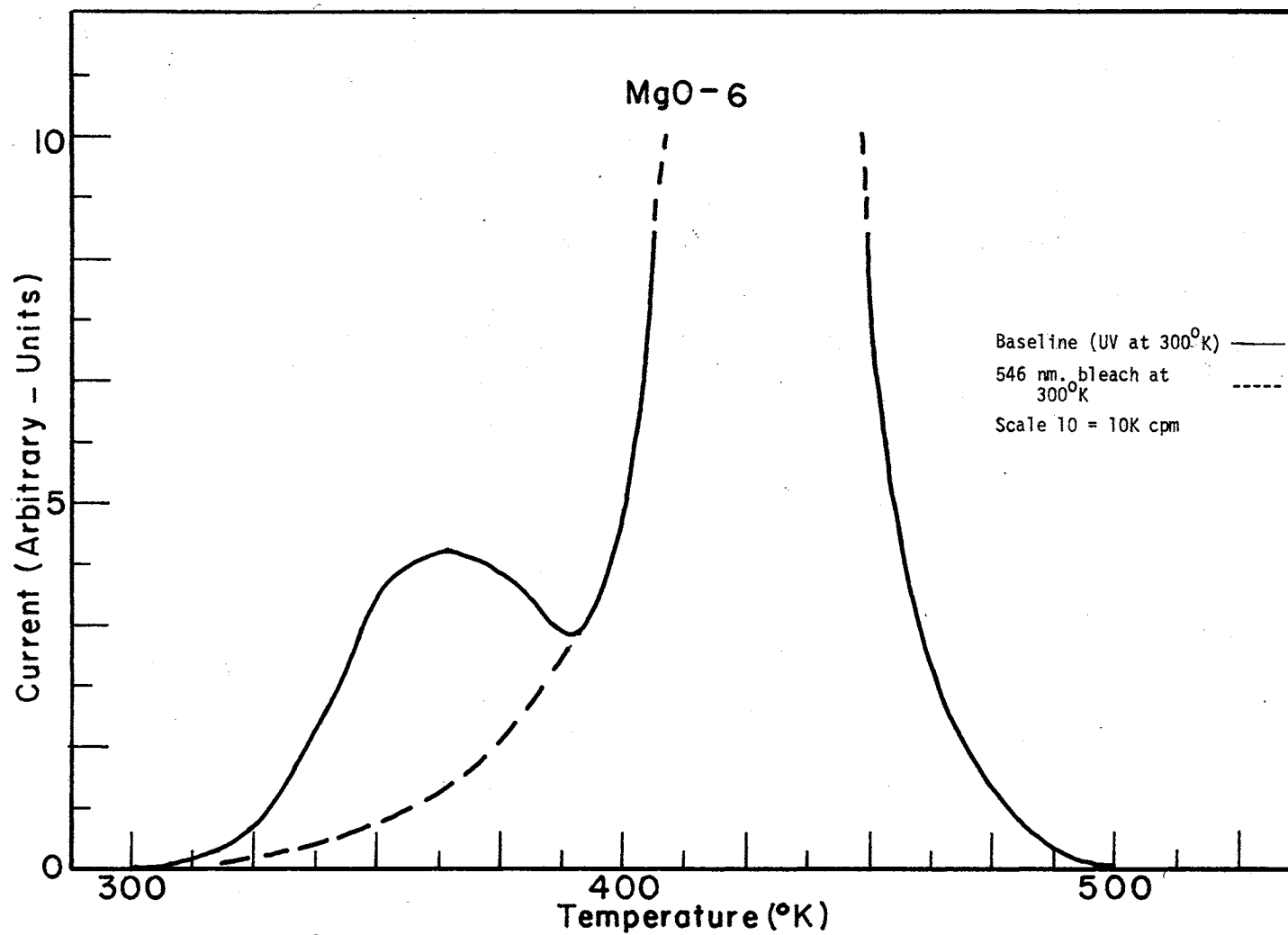


Figure 15. 546 Nanometer Bleaching of T.S.C.E. From MgO-6 at 300°K

peak. This peak was not noticeable in the gas system while it shows up for all of the samples in the high vacuum system. Further discussion concerning this peak will be delayed until Chapter V.

Figure 16 corresponds to the effect on T.S.C.E. of following a 34 minute full band ultraviolet excitation at room temperature by 2 hours of focused 546 nanometer light near 77°K . The solid curve represents the baseline run of ultraviolet excitation alone, while the dashed curve represents the effects of bleaching. Two hours of focused 546 nanometer light by itself does not produce any measurable charge emission or luminescence using the most sensitive signal to noise measurements, and as expected the baseline run does not produce any peak structure below room temperature. As the dashed curve indicates, the bleaching light produces structure near 200°K and 236°K and partially bleaches the peak near 361°K . The peak near 439°K seems to have decreased a little after the bleach.

Figure 17 represents the simultaneous luminescence runs with the bleaching light producing some observable structure near 200°K and decreasing the peak intensity near 361°K . Again the baseline run shows no peak structure below room temperature.

Using 254 nanometer light in place of the 546 nanometer excitation mentioned above produces the results indicated in Figure 18. The solid curve represents the baseline run after the full band irradiation at 300°K while the dashed curve illustrates the effect of following the room temperature excitation with 254 nanometer light near 77°K . The results suggest no bleaching effects (except for the peak near 440°K). Instead, as the circled curve implies, the effect of the 254 nanometer excitation by itself near 77°K is to produce all of the peak structure,

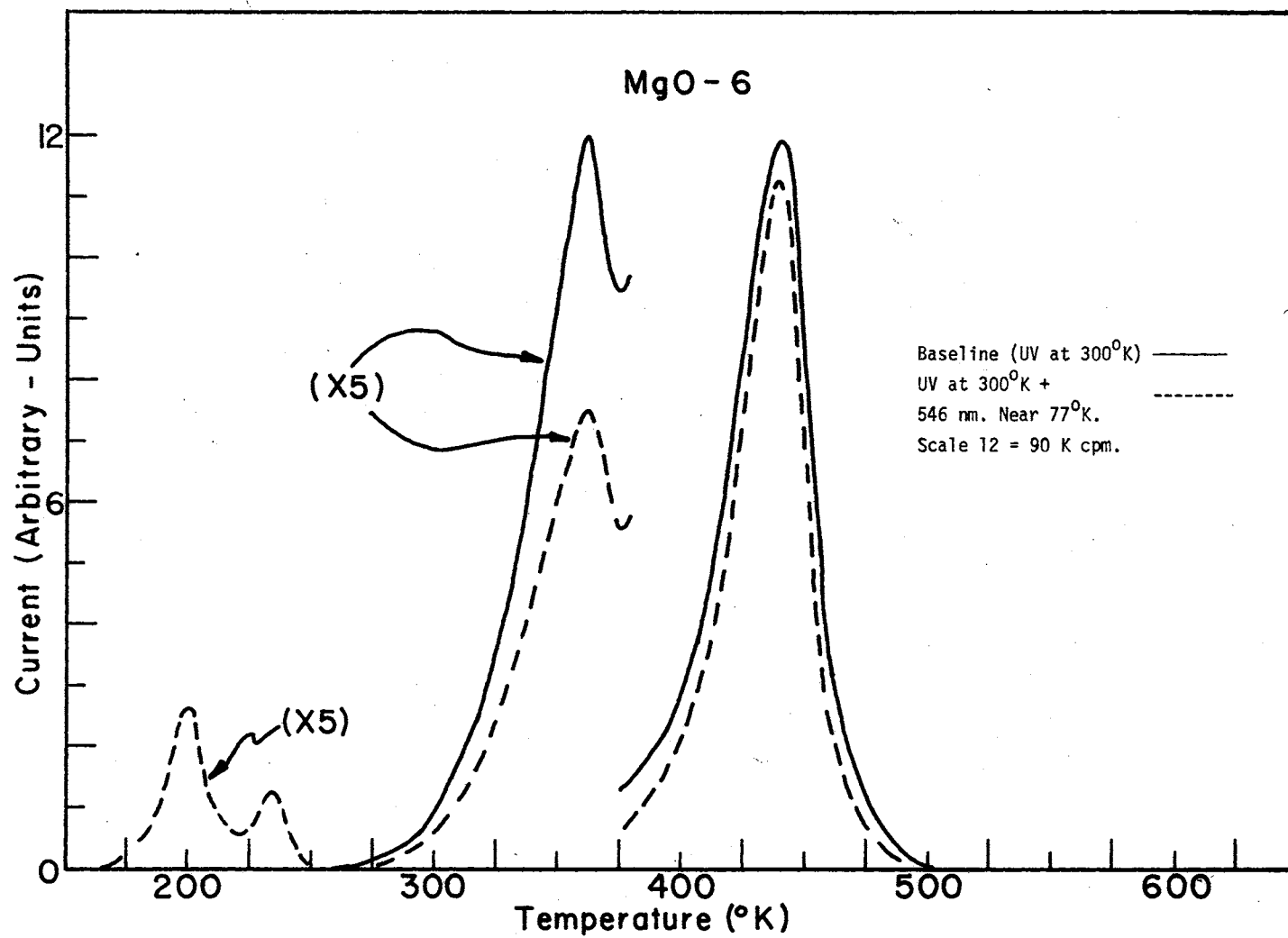


Figure 16. 546 Nanometer Bleaching of T.S.C.E. From MgO-6 Near 77°K

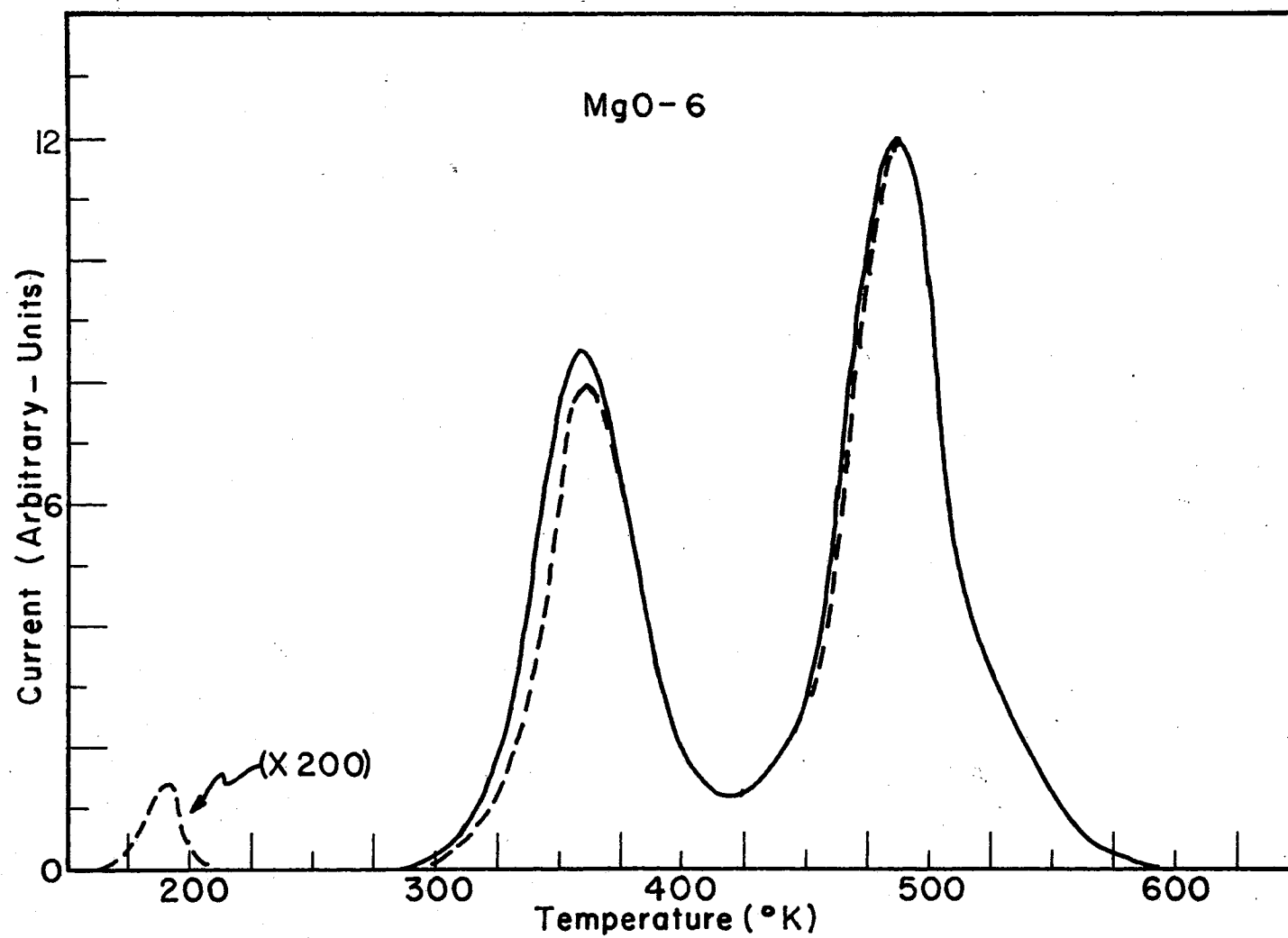


Figure 17. 546 Nanometer Bleaching of T.S.L. From MgO-6 Near 77°K

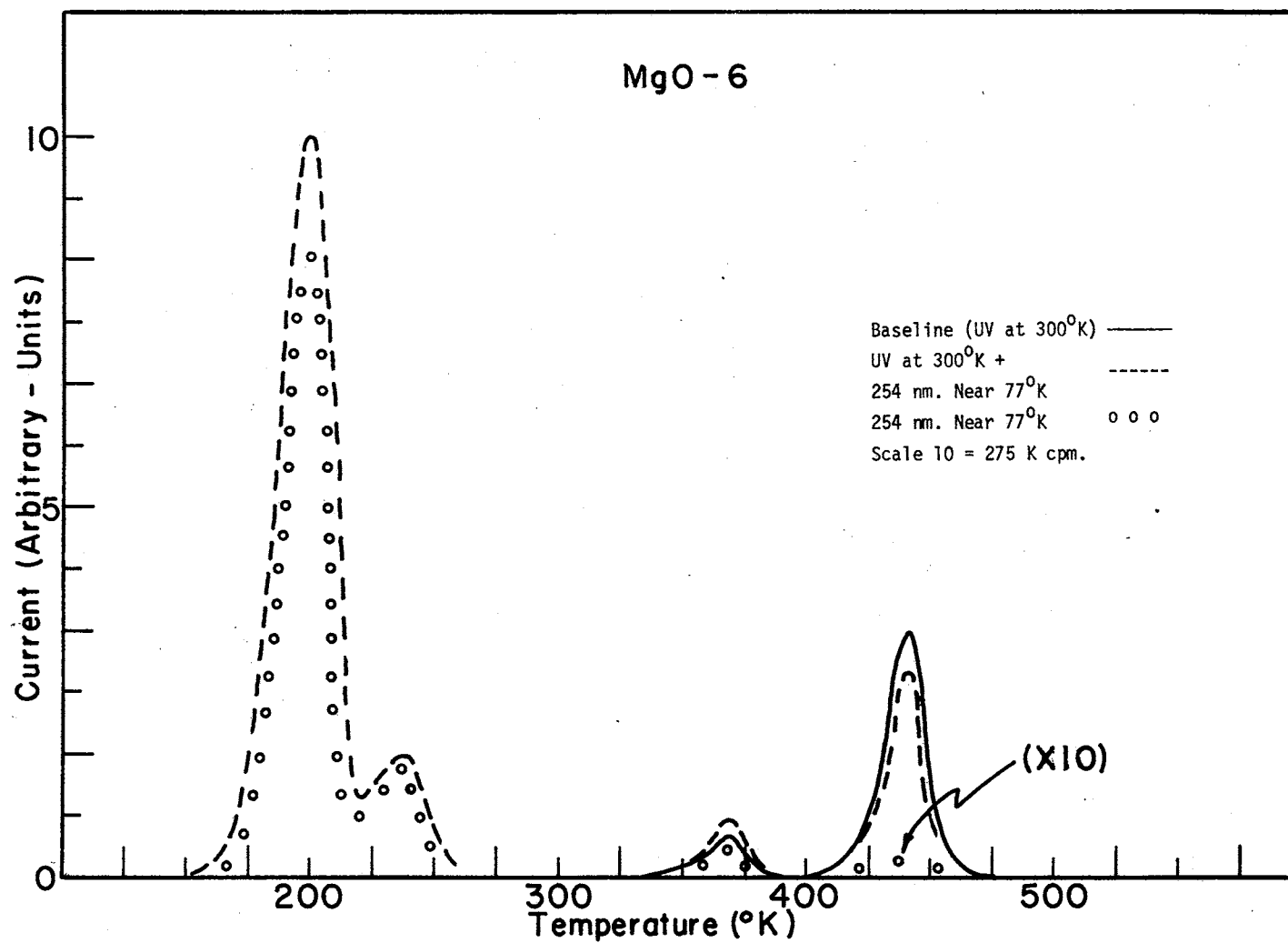


Figure 18. 254 Nanometer Re-excitation of T.S.C.E. From MgO-6

especially that below 300°K .

The corresponding luminescence is represented in Figure 19 where the solid curve is indicative of the full band excitation at room temperature followed by 254 nanometer light near 77°K . The dashed curve represents the effect of the 254 nanometer light by itself near 77°K . The double excitation run shows more intense structure near 200°K and less intensity near 234°K . Comparing this with the dashed curve implies that no bleaching seems to occur and that the 254 nanometer irradiation populates the shallow traps associated with the peak near 200°K like the full band excitation does after gamma ray treatment at room temperature (Figure 14).

Excitation with 313.0 nanometer light by itself produces characteristic charge emission near 200°K and 236°K and small peaks above room temperature. The luminescence results are very similar in intensity to the peak structure of the dashed curve of Figure 19.

Gamma irradiating MgO at room temperature and then subjecting it to either 546, 440, 313 or 254 nanometer light near 77°K produces an enhancement of both peaks near 188°K and 235°K with the former peak being enhanced more. This same effect was observed in Figure 14 but not with individual bands of excitation from the mercury lamp.

All of the above re-excitation indicates that charge is being transferred from deep traps to shallow traps that are stable near 77°K .

T.S.C.E. Peak Intensity Changes

Throughout the charge emission runs in the gas system, it was noticed that the peak in the vicinity of 310°K would increase from approximately 0.5 the intensity of the peak near 364°K in the initial run to

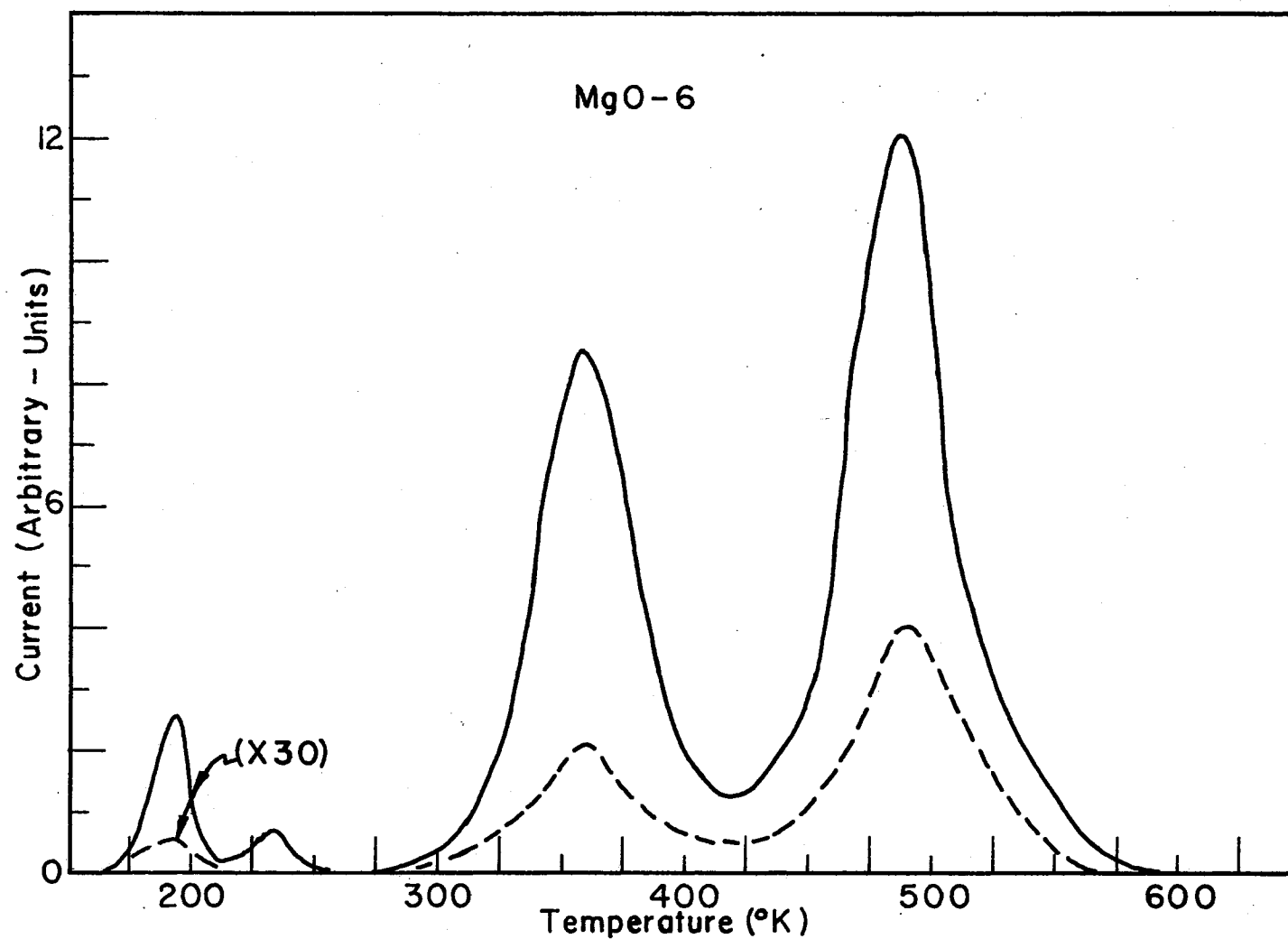


Figure 19. T.S.L. From MgO-6 After 254 Nanometer Excitation Near 77°K

approximately the same intensity and sometimes larger with the second and third consecutive runs. Figure 20 illustrates this with the initial experiment indicated by the solid curve and the second by the dashed curve. Once the first two initial runs are completed the peak structure remains more stable. When the peaks have reached this equilibrium state it is convenient to check the effects of gas adsorption on charge emission. An O_2 gas purge was then performed (following above initial runs) after the system had been evacuated with the liquid nitrogen copper trapped diffusion pump and then isolated with the high vacuum valve. This maintained a vacuum of 5×10^{-5} Torr. The O_2 gas was then introduced until a pressure near 1 atmosphere was obtained. The system was then evacuated through the liquid nitrogen trap with the forepump. At this point the counting gas was readmitted. The dashed-circle curve was then produced indicating that O_2 gas enhances both peaks. Another run immediately after this reduces the peaks back to near the dashed curve again. The low temperature peaks, which are not indicated, were not affected appreciably by the O_2 purge at $300^\circ K$. A plausible explanation for this is that the forepump evacuation removes all of the weakly adsorbed purging gas that could affect the low temperature structure, while that above $300^\circ K$ is affected by the remaining more stable adsorption states of O_2 .

All of the high vacuum runs to be discussed next were made with the vacuum pump effects removed (previous section). The effects of adsorbed gas are illustrated in Figure 21 implying that the peak intensities decrease after several runs in the high vacuum system. The solid curve represents an initial run, with the remaining curves being indicative of runs made several days later. As expected, more runs produce a better

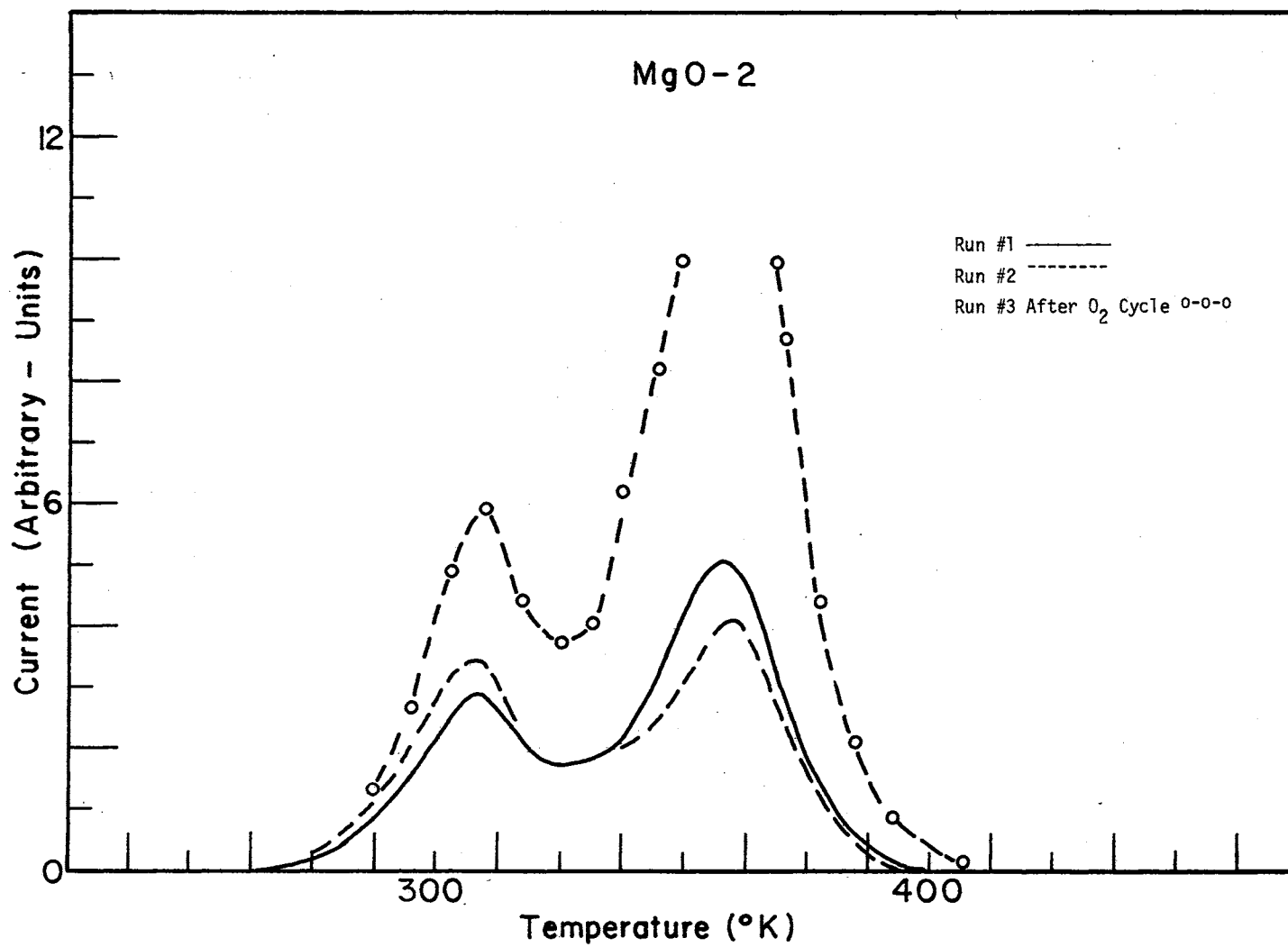


Figure 20. T.S.C.E. Intensity Changes in the Gas System

vacuum and a cleaner MgO surface. If the system is purged with either dry oxygen or dry nitrogen gas at 300°K , the original intensity is again produced while the peaks below 300°K are not appreciably affected. Runs immediately following the gas purging run reduce the peak intensities back to the dotted curve. The major effect of the gas is the peak enhancements and no major shift in the peak positions with respect to temperature. Similar effects were observed if a crystal was submerged in distilled H_2O for several hours and then dried with a Kimwipe before placing the sample back into the high vacuum system.

Figure 21 also implies that the low temperature peak structure is more intense than the above 300°K structure, while Table I illustrates the opposite. The latter represents data from the gas system, and a possible explanation for this apparent conflict is that the counting gas molecules have a low mobility below room temperature, which means that smaller electron avalanches are produced in the vicinity of the anode yielding a smaller current. Smaller charge emission energies would also produce a similar effect.

The peak enhancement near 310°K that is illustrated in Figure 20, (compare dashed and solid curves) but not in Figure 21, was again observable when the $\text{MgO}:\text{H}_2\text{O}$ run mentioned above was made. That this peak enhancement was present in the gas system, and not as obvious in the regular high vacuum runs, could be associated with the presence of H_2O for the initial runs in the gas system, while in the high vacuum system H_2O desorption is more pronounced. It should also be noted that as more runs are made in vacuum, the peak near 310°K appears to decrease more rapidly and eventually becomes almost undetectable. This is also true of peaks that appear at higher temperatures in the vicinity of 478°K and

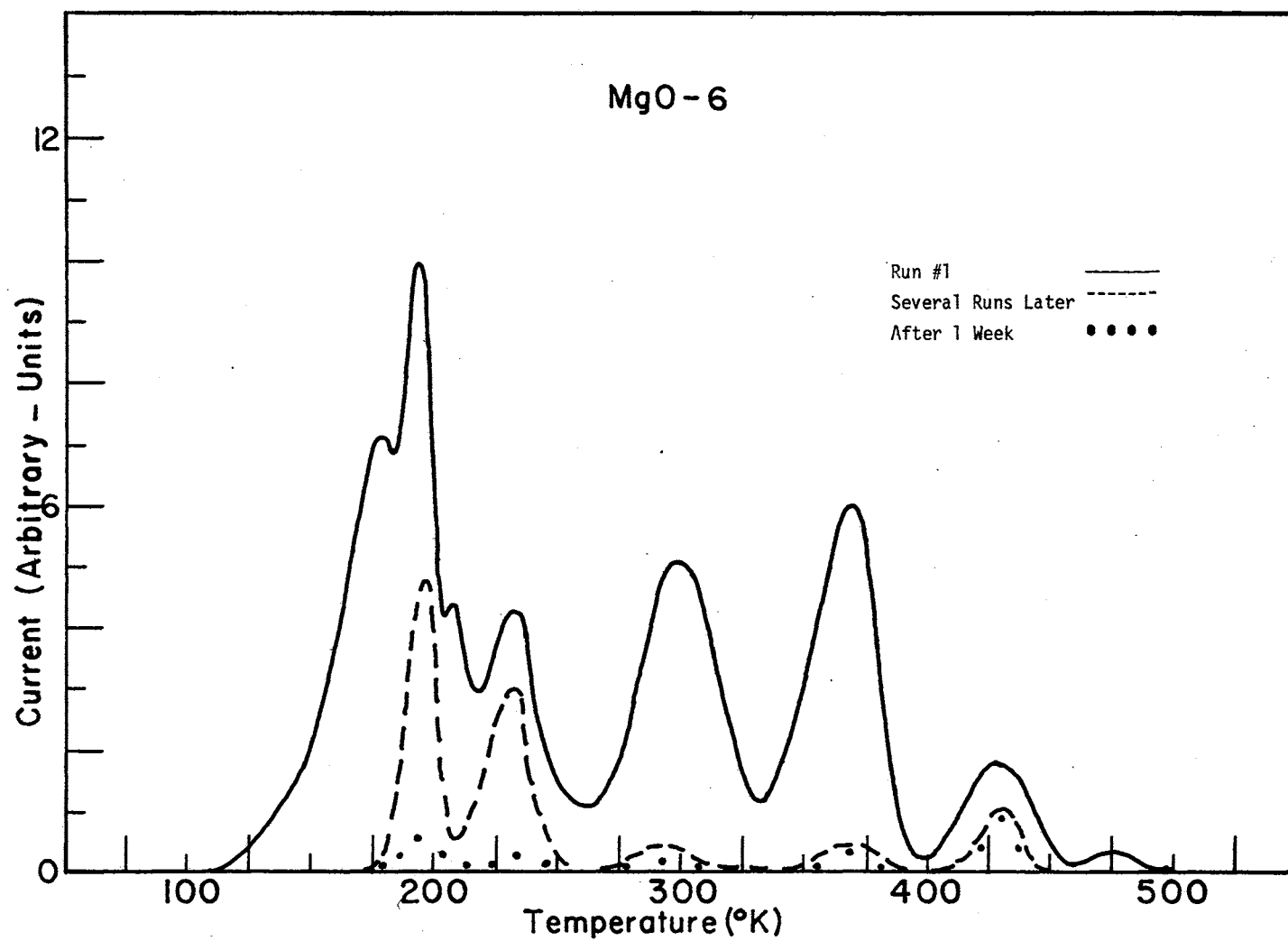


Figure 21. T.S.C.E. Intensity Changes in the Vacuum System

higher, again suggesting adsorption desorption effects. Only the high temperature (\geq vicinity of 478°K) peaks in the gas system disappeared gradually after several runs. Even though the charge emission decreased after a period of runs extending over a week in the vacuum, the luminescence (1P28) seemed to remain stationary (within experimental error). A detailed discussion of the above gas effects is presented in Chapter V.

Magnetic Field and Grid Voltage Effects on T.S.C.E.

The presence of a 75 gauss field (measured between the sample and grid) reduces all of the charge emission peaks by an average 80%, regardless if the field is present after initial or final runs in the vacuum system. If the field is applied after several runs the effect appears to be even better. This is attributed to the fact that a good homogeneous field was hard to produce in the vicinity of the sample because of the geometry of the system. A field of 75 gauss should be sufficient to produce a radius of curvature of 0.5 cm. if the accelerating voltage is near 150 volts and the charge emission consists of electrons. If the emission consisted of ions no major deflection would occur and there would be no intensity changes. Since a grid voltage of +300 volts was used and the distance from the sample surface to the grid is approximately 1 cm., the average accelerating voltage is +150 volts which implies that at least 80% of the charge emission consists of electrons.

No major difference in charge emission is noticed if the grid voltage is reduced from the regular +300 volts to +150 volts in the vacuum runs. If the grid voltage is completely removed, and the vacuum pump effects cleared, it is noticed that the predominant peak that remains is the one near 380°K . This implies that the charge released at this

temperature is more energetic than the other charge emissions. This was also observed in the gas system where a grid was placed over the opening in the stainless steel cylinder. A negative voltage of several volts with respect to the sample was needed in order to reduce the emission peak mentioned above. It was also noted that a positive voltage enhanced this peak but would not produce the low temperature peaks.

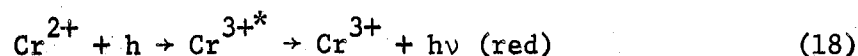
CHAPTER V

DISCUSSION AND CONCLUSIONS

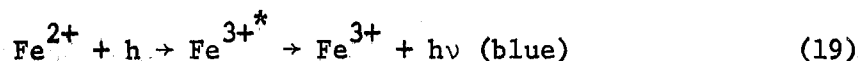
T.S.L. and Hole Centers in MgO

E.S.R. has positively identified the presence of the V^- center in all of the MgO samples, after either gamma or ultraviolet irradiations, and has shown that subsequent heating to near 383°K anneals this color center and also that Fe^{3+} and Cr^{3+} concentrations increase. Also, bleaching experiments, similar to that illustrated by Figure 18 and others at room temperature with 546 nanometer light, support the idea of the destruction of the V^- center, for this is thought to be the most efficient bleaching agent for these centers (26).

Wertz, et. al. (60) have identified the decay of the V^- center near 383°K with the following reaction



while Sibley et. al. (30) concur with this, and also propose that the additional blue emission of light they observed in the same temperature region was from the reaction



That both the blue and the red emission of light occur near 383°K from MgO-6, MgO-2 (Figures 13, 32 and 42) and also from MgO-3 (T.S.L.

checked through filters) indicates that similar reactions are occurring in these crystals. Since Figure 11 demonstrates that similar emissions of light occur (blue and red) in the 383°K and 500°K regions for MgO-6, and E.S.R. shows a corresponding change in Fe^{3+} and Cr^{3+} in both temperature regions, it is possible that a hole release mechanism is occurring in the vicinity of 500°K . Mallard and Crawford's (33) thermal electric power measurements indicate hole conduction above 383°K , while Peria's (61) photoconductivity results associate a hole-release peak with 310 nanometer absorption. Since Figure 12 shows the Mn^{2+} concentration decreasing in the 500°K region it is tempting to associate the possible hole release with this change, but Mn^{1+} would be the end result, which isn't very plausible for this high temperature.

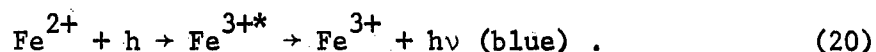
Chao (62) has suggested that a broad emission band superimposed on the 720 nanometer Cr^{3+} thermoluminescence is associated with Mn^{2+} , while Ziniker et. al. (63) have associated Mn^{2+} with 620 nanometer emission from MgO. As Figure 11 indicates, there neither seems to be a presence of Chao's broad emission band or the 620 nanometer emission that Ziniker has mentioned, while E.S.R. (Figure 12) shows a changing Mn^{2+} concentration. It should be pointed out that the emission spectroscopy data is representative of crystals that have the largest luminescence in the 500°K range (e.g., MgO-6), while MgO-2 and MgO-3 emission spectroscopy studies were not performed because their emissions in the temperature range are much smaller. Hecht and Taylor (64) saw a luminescence peak near 500°K in MgO powders and attributed it to Cu^{2+} . MgO-6 does have a Cu^{2+} E.S.R. signal (MgO-2 and MgO-3 had no observable Cu^{2+} E.S.R. signal), but detailed analysis before and after excitation showed no change in the Cu^{2+} spectra observed near 77°K .

There is also the presence of non-paramagnetic ions that can act as traps or recombination centers. A hole could be released from a trap associated with such an impurity, giving the characteristic emission observed for the Fe^{3+*} and Cr^{3+*} excited state decays to their ground states while also converting the Mn^{2+} to Mn^{3+} .

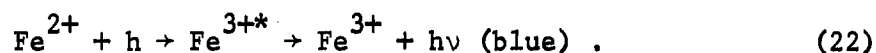
The 309°K luminescence peak in Figure 14 occurs in the temperature range where the V_{OH} decay has been observed by Kirklin et. al. (70). If this peak is associated with the V_{OH} center then its intensity implies that it should be observable with E.S.R. near 77°K . This has been experimentally verified. Kappers and Wertz (69) have demonstrated that the annealing of the V_{OH} center can produce more V^- centers by the re-trapping of holes which are released by the decaying V_{OH} center. That this peak was observable with the 7102 photomultiplier implies that the emission is just in or above the upper spectral sensitivity limit of the 1P28 (≈ 800 nanometers). It is therefore possible that the hole released from this center recombines with Cr^{3+} producing the characteristic red emission of light associated with the Cr^{3+*} decay (60). Since its thermoluminescence was approximately 0.1 the intensity of that produced by the V^- decay, its emission spectroscopy was not obtained. In addition, the temperature range where the V_{OH} center is thought to thermally decay (near 309°K), and its overlap with the thermal decay of the V^- center near 383°K would have also prevented a good observation of the spectral distribution of the former center.

The luminescence peaks below 300°K were always very small unless optically re-excited after gamma irradiation at room temperature. Hecht and Taylor (64) observed T.S.L. near 188°K and 235°K , while their filter analysis showed emissions in the ranges of (345 - 480) nanometers and

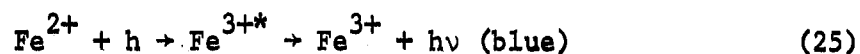
(480 - 385) nanometers respectively. Filter checks of the thermoluminescence (1P28 observation) from MgO-3, after gamma irradiation at 300°K and optical re-excitation near 77°K, showed that the wavelength emission of the 200°K peak agreed with their (345 - 480) nanometer observation, while that of the 235°K peak appeared closer to a 380 nanometer spectral distribution. That the low temperature T.S.L. was observable with both the 1P28 (predominantly blue spectral sensitivity) and the 7102 (red and blue spectral sensitivities), indicates that the above mentioned filter checks are reasonably accurate. This then implies a spectral distribution similar to that near 383°K where a possible reaction is



The E.S.R. showed that Fe^{3+} decreases, if after gamma irradiation at 300°K the sample is excited with the full band of ultraviolet light near 77°K. Attempts to associate valence changes with the 188°K and 235°K luminescence peaks by annealing experiments with the E.S.R. system failed, but as Figure 15 illustrates the low temperature T.S.L. structure is at least a factor of 200 less than that near 383°K, implying that the low temperature valence changes could be beyond the limits of the sensitivity of the E.S.R. system. Similarly, no significant signal for V° centers was detectable near 77°K, but again if they are associated with the low temperature luminescence peaks their concentration could be approximately 200 - 250 times less than that of the V^{-} center (by comparing T.S.L. intensities in Figure 15). Since V° centers are unstable at 300°K and can be produced by ultraviolet or gamma irradiation near 77°K (25, 26), a possible reaction producing a low temperature luminescence would be the following:



This would occur after irradiation near 77°K and during subsequent heating to 300°K. A similar reaction might exist where the V^{-} center (produced by excitation at 300°K) is converted to the V° center by a second excitation near 77°K. The following reactions could then be possibilities for producing thermoluminescence below 300°K.



All wavelengths from 546 nanometers to 254 nanometers were experimentally capable of optically re-exciting the low temperature peaks. There is also the possibility that other deeper unidentified hole centers exist from which shallow hole traps could be filled, or that the luminescence could be associated with electron traps in a similar manner. The fact that the low temperature T.S.L. is almost insignificant with respect to that above 300°K agrees with the idea of a low concentration of V° centers produced near 77°K. Since it is known that V° centers can be converted to V^{-} centers (65) it is very plausible that the V° center is associated with the luminescence below 300°K.

Charge Emission From MgO

The bleaching effects of the 546 nanometer light on the charge emission (Figures 16 and 17) near 370°K, suggest that the hole released

from the V^- center is associated with the T.S.C.E. A plausible model for the T.S.C.E. in this temperature region is provided by the Auger mechanism. This model is a possible explanation for all of the charge emission that occurs near luminescence peaks associated with the release of holes as with the V^- , V_{OH} and the V^0 centers in MgO. Since the high vacuum and the gas systems indicated the effects of O_2 , N_2 , H_2O and O_2 respectively on the MgO surface with respect to charge emission, it is possible that when a hole is released from the V^- center it recombines with an impurity near the surface, with the recombination energy being transferred to a nearby gas molecule that is chemically attached to another imperfection, with the subsequent emission of the electron that allowed for the sorption. Another example would be the recombination of the hole with one impurity that has adsorbed a gas molecule, while the recombination energy liberates the adsorbed molecules and an associated electron. This would explain the tremendous decrease of the charge emission in the vacuum, and also the necessary energy needed for the T.S.C.E. This does not mean that the Auger model can only be used as a working method for explaining charge emission when adsorbed gas is present, but that with MgO, the presence of gas tends to increase rather than hinder the charge emission. Since gas desorption seems to affect the peak intensities, there should exist the possibility of detecting a change in pressure near the emission peaks. There was a corresponding change in pressure ($\Delta p \approx 3 \times 10^{-6}$ Torr) with the 190°K T.S.C.E. The pressure increase would occur with the initial rise of the charge emission. This change in pressure was determined with, and without, a sample in the high vacuum system. The pressure changes for the remaining peaks could not be checked as closely, for the outgassing of the system would steadily in-

crease above 300°K , preventing accurate measurements of Δp .

That the emission peak near 311°K would at first increase, and then gradually decrease more rapidly with respect to the peak near 375°K (Figure 22), is not explained very well by the gas desorption. A possible explanation for this is that the adsorbed H_2O is gradually being converted to hydroxyl groups, with the hydrogen diffusing into the Mg^{2+} vacancies and allowing for the possible creation of V_{OH} centers, which then break down more with further heating, ultraviolet excitation and high vacuum treatment. Anderson et. al. (66) suggest that H_2O consists of a hydroxyl group adsorbed on a powdered MgO surface cation, and the remaining hydrogen forming another hydroxyl group with an adjacent surface O^{2-} ion after annealing the powder in a high vacuum. According to Anderson et. al., the optical absorption of these centers grows after partial H_2O desorption from the powdered MgO surface near 523°K . After several anneal runs near 775°K , one of the hydroxyl groups' optical absorption bands starts to disappear more rapidly than the other and eventually decreases to a low level. Since Braunlich (67) has suggested that charge emission can occur from discrete areas of a surface, it would seem very plausible for this hydroxyl formation to exist on MgO at discrete sites and react as a dipole, with the proton from the hydrogen setting up a positive field for the charge emission. This would explain the initial increase of the charge emission near 311°K , and then its rapid decay in the high vacuum system, while in the gas system the replenishment of OH groups would prevent such an occurrence.

Activation Energy Analysis

The initial rise and the Balarin-Zetsche methods were used for the

activation energy analysis giving values of 1 and 0.85 eV for the charge emission peaks near 370 and 309°K respectively. These values agree reasonably well with Chao's value (62) of 0.8 eV for the hole release of the V^- center and also Kirklin's (70) value of 0.84 eV for the hole release of the V_{OH} center. An average value of 0.76 eV was obtained for the T.S.C.E. below 300°K, which appears too high, especially for peaks in the temperature range of 200°K. That the values for the low temperature peaks are high is rather surprising, since the charge emission curves obtained from the gas system were analyzed where the peaks below 300°K were well resolved in structure, while the 370°K peaks had to be isolated by annealing through 311°K, cooling back and then continuing the heating rate before the overlapping of the two peaks was removed. The use of the Balarin-Zetsche method could be questioned because it is designed for essentially first order kinetics, where it is assumed that no significant retrapping occurs. However, the use of the initial rise method is more independent of the order of the kinetics (first or second order) and its use also produced high values. Since the heating rates through the peak temperature ranges were linear, no further comment can be made until further analysis and techniques are applied.

Summary

The majority of the charge emitted from MgO single crystals is composed of electrons suggesting that the terminology of thermally stimulated electron emission is more appropriate, while the decay of the hole centers V_{OH} and V^- near 311 and 375°K respectively, supports the idea of the Auger mechanism as a working model for explaining the electron emission in these temperature ranges. It is plausible that the V^0 hole

center is associated with the low temperature luminescence and charge emission, but further experimentation will have to be performed on crystals with V° concentrations detectable with E.S.R., in order to determine a more exact temperature at which this center decays before further correlation can be made with T.S.L. and T.S.E.E.

That the minor charge emission from some crystals at temperatures above 475°K would gradually disappear, after repeated runs in the gas system, implied that the release of electrons was associated with adsorption-desorption effects, which could also be produced by an as yet unidentified hole release as the spectral distribution of MgO-6 in Figure 11 and its summary in Table II indicate. Similarly, the corresponding E.S.R. data in Figure 12 support the idea of a release of holes near 500°K .

Suggestions for Further Study

Since it is believed that the hole centers play an important part in the electron emission, crystals with high V_{OH} concentration should be observed by optical absorption and the V_{OH} concentration correlated with the corresponding charge emission near 311°K . A check for obtaining more V^{-} centers from V_{OH} centers (69) was experimentally performed with the charge emission with no definite results, but additional experiments similar to this should be tried with both the T.S.E.E. and the T.S.L. for further experimental evidence for the Auger method as a working model for T.S.E.E.

Wertz et. al. (71) have suggested that heating MgO in oxygen at 1473°K for 2 hours and then irradiating near 77°K , produces a two orders of magnitude increase in the V° center. This would enhance the low tem-

perature electron emission and thermoluminescence if Equations (24) and (25) are correct.

Thermal electric power measurements could possibly help resolve whether or not a deep hole is associated with the luminescence and weak electron emission near 500°K .

Preliminary E.S.R. experimentation on a lightly neutron irradiated crystal has shown that F^{+} and V^{-} centers exist while T.S.L. indicated major structure above and below 300°K . Since there was also corresponding major T.S.E.E. structure it would be beneficial to study crystals of this nature in more detail in order to determine if a possible reaction exists where the release of a hole from the V^{-} center annihilates an electron of the F center (F^{+} converted to F by ultraviolet excitation) producing thermoluminescence while the competing non-radiative process near the surface (Auger method) produces charge emission from O_2^{-} adsorbed at the F center (28). Further experimentation on lightly neutron irradiated crystals might also alleviate the identity of the T.S.E.E. peak that appeared near 440°K in the vacuum system for a major T.S.L. peak occurred from this crystal at 440°K with corresponding T.S.E.E. structure.

REFERENCES

- (1) Lewis, W. B. and Burcham, W. E., Proc. Camb. Phil. Soc., 32, 503 (1936).
- (2) Grunberg, L., Brit. J. Appl. Phys., 9, 85 (1958).
- (3) Grunberg, L. and Wright, K. H. R., Proc. Roy. Soc. (London), 232, 403 (1955).
- (4) Pimbley, W. T. and Francis, E., J. Appl. Phys., 32, 1729 (1961).
- (5) Scharmann, A. and Seibert, G., Z. Phys., 183, 249 (1965).
- (6) Ramsey, J. A., J. Appl. Phys., 37, 452 (1966).
- (7) Gesell, T. F., Arakawa, E. T. and Callcott, T. A., Surface Science, 20, 174 (1970).
- (8) Dreuckhan, J., Gross, H. and Glaefcke, H., Phys. Stat. Sol. (a), 2, K 201 (1970).
- (9) Drenckhan, J., Gross, H. and Glaefcke, H., Phys. Stat. Sol. (a), 2, K 51 (1970).
- (10) Garlick, G. F. J. and Gibson, A. F., Proc. Roy. Soc. (London), A60, 574 (1948).
- (11) Braunlich, P., Paper in Proceedings of the Conference on the Applications of Thermoluminescence to Geological Problems, Spoleto, Italy (1966).
- (12) Kelly, P. and Braunlich, P., Phys. Rev. B, 1, 1587 (1970).
- (13) Kelly, P., Laubitz, M. J. and Braunlich, P., Phys. Rev. B, 4, 1960 (1971).
- (14) Lepper, J., Z. Naturforsch., 10a, 47 (1955).
- (15) Navotney, A., Spurney, Z. and Binova, M., J. Phys. Chem. Solids, 31, 1412 (1970).
- (16) Holzapfel, G., Phys. Stat. Sol., 33, 235 (1969).
- (17) Gaprindoshvily, A. Y. and Kortov, V. S., Phys. Stat. Sol. (a), 4, K 231 (1971).

- (18) Bichevin, V. and Kaambre, H., Phys. Stat. Sol. (a), 4, K 235 (1971).
- (19) Tolpygo, E. I., Tolpygo, K. B. and Sheinkman, M. K., Akademiia Nauk SSSR Bulletin Physical Series, 30, 1980 (1966).
- (20) Kelly, P., Phys. Rev. (in press).
- (21) Becker, K., Atomic Energy Review, 8, 173 (1970).
- (22) Bohun, A., Czeck, J. Phys., B10, 360 (1960).
- (23) Bohun, A. and Kaambre, H., Czech. J. Phys., B14, 54 (1964).
- (24) Reiling, G. H. and Hensley, E. B., Phys. Rev., 112, 1106 (1958).
- (25) Hughes, A. E. and Henderson, B., Defects in Solids (to be published).
- (26) Henderson, B. and Wertz, J. E., Adv. Phys., 17, 749 (1968).
- (27) Krylova, I. V., Phys. Stat. Sol. (a), 7, 359 (1971).
- (28) Nelson, R. L., Hale, J. W. and Harmsworth, B. J., Far. Soc. Trans., 67, 1164 (1971).
- (29) Wong, Ning-Bew and Lunsford, Jack H., J. Chem. Phys., 55, 3007 (1971).
- (30) Kolopus, J. L., Mallard, W. C. and Sibley, W. A., Phys. Stat. Sol., 31, 223 (1969).
- (31) Chao, C. C., J. Phys. Chem. Solids, 32, 2517 (1971).
- (32) Ziniker, W. M. and Merrow, J. K., J. Phys. Chem. Solids (in press).
- (33) Mallard, W. C., and Crawford, J. H., Jr., J. Phys. Chem. Solids (in press).
- (34) Gordon, P., Scharmann, A. and Seibert, J., Phys. Stat. Sol., 33, K 97 (1969).
- (35) Maenhout, W. and De Muer, D., Physica, 49, 157 (1970).
- (36) Kriegeis, W. and Scharmann, A., Phys. Stat. Sol., 33, K41 (1969).
- (37) Kriegeis, W. and Scharmann, A., Z. Naturf., 24a, 862 (1969).
- (38) Bohun, A., Czeck. J. Phys., 5, 64 (1955).
- (39) Braunlich, P., J. A. P., 38, 2516 (1967).
- (40) Balarin, M. and Zetsche, A., Phys. Stat. Sol., 2, 1670 (1962).

- (41) Korff, S. A., Electron and Nuclear Counters, D. Van Nostrand Company, Inc., New York (1955).
- (42) Diethorn, W. A., A Methane Proportional Counter System for Natural Radiocarbon Measurements, NYO-6628, March 16, 1956.
- (43) Kiser, R. W., Applied Scientific Research, 8, 183 (1960).
- (44) Kiser, R. W. and Storrs, C. D., Applied Scientific Research, 8, 387 (1960).
- (45) Bohun, A. and Dolejši, J., Czech. J. Phys., 9, 578 (1959).
- (46) Bohun, A., Acta phys. Austriaca, 10, 353 (1957).
- (47) Tolpygo, E. I., Tolpygo, K. B. and Sheinkman, M. K., Soviet Physics Solid State, 7, 1442 (1965).
- (48) Krylova, I. V. and Kупenko, O. G., Russian Journal of Physical Chemistry, 40, 1570 (1966).
- (49) Rakhmatullina, I. A. and Krylova, I. V., Russian Journal of Physical Chemistry, 42, 1407 (1968).
- (50) Krylova, I. V. and Rodina, I. A., Russian Journal of Physical Chemistry, 45, 660 (1971).
- (51) Krylova, I. V., Minchev, Kh. and Penchev, V., Russian Journal of Physical Chemistry 45, 874 (1971).
- (52) Moglich, F. and Rompe, R. W., Z. Physik, 115, 707 (1940).
- (53) Goodman, B., Lawson, A. W. and Schiff, L. I., Phys. Rev., 71, 191 (1947).
- (54) Curie, D., J. Phys. et Radium, 12, 920 (1951).
- (55) Kubo, R., Phys. Rev., 86, 929 (1952).
- (56) Haung, K. and Rhys, A., Proc. Roy. Soc. (London), A204, 406 (1950).
- (57) Vasileff, H. D., Phys. Rev., 96, 603 (1954).
- (58) Becker, Klaus, CRC Critical Reviews in Solid State Sciences, 3, 39 (1972).
- (59) Crase, K. W., Becker, K. and Gammage, R. B., ORNL-TM-3572, (1971).
- (60) Wertz, John E., Hall, L. C., Helgeson, J., Chao, C. C. and Dykoski, W. S., Interaction of Radiation With Solids, Plenum Press, New York (1967).
- (61) Peria, W. T., Phys. Rev., 112, 423 (1958).

- (62) Chao, C. C., J. Phys. Chem. Solids, 32, 2517 (1971).
- (63) Ziniker, W. M., Merrow, J. K. and Mueller, J. L., J. Phys. Chem. Solids, 33, 1619 (1972).
- (64) Hecht, H. G. and Taylor, E. D., J. Phys. Chem. Solids, 28, 1599 (1967).
- (65) Private communication with Lawrence A. Kappers, Oklahoma State University, Stillwater, Oklahoma.
- (66) Anderson, P. J., Horlock, R. F. and Oliver, J. F., Trans. Faraday Soc., 61, 2754 (1965).
- (67) Braunlich, P., J. Appl. Phys., 42, 495 (1970).
- (68) Ghosh, T. K. and Clarke, F. J. P., Brit. J. Appl. Phys., 12, 44 (1961).
- (69) Kappers, L. A. and Wertz, John E., Solid State Communications 9, 1755 (1971).
- (70) Kirklin, Perry W., Auzius, Peteris and Wertz, John E., J. Phys. Chem. Solids, 26, 1067 (1965).
- (71) Wertz, John E., Auzius, Peteris, Griffiths, J. H. E. and Orton, John W., Disc. Faraday Soc., 28, 136 (1959).

VITA 2

Howard Charles Mollenkopf

Candidate for the Degree of

Doctor of Philosophy

Thesis: A STUDY OF THERMALLY STIMULATED CHARGE EMISSION AND THERMALLY STIMULATED LUMINESCENCE FROM MgO SINGLE CRYSTALS

Major Field: Physics

Biographical:

Personal Data: Born in Cisco, Texas, April 6, 1940, the son of Mr. and Mrs. George Mollenkopf, Sr.

Education: Graduated from Sacred Heart High School, Muenster, Texas, May, 1958; attended the University of Texas, Austin, Texas, from 1958 to 1960; Gainesville Jr. College, Gainesville, Texas, 1960; North Texas State University, Denton, Texas, 1960-1964, received the Bachelor of Science degree in 1964, with a major in Physics; received the Master of Science degree in 1967, with a major in Physics; attended Oklahoma State University in 1968; completed the requirements for Doctor of Philosophy degree in May, 1973.

Professional Experience: Graduate Teaching Assistant, Physics Department, North Texas State University, 1964-1966; Instructor in Physics, Kansas State Teachers College, Emporia, Kansas, 1966-1968; Graduate Teaching Assistant, Physics Department, Oklahoma State University, 1968-1970; National Science Foundation Research Trainee, Physics Department, Oklahoma State University, 1970-1972.